

# Global Biogeochemical Cycles

## RESEARCH ARTICLE

10.1029/2019GB006505

### Key Points:

- Spatial allocation and high instrumental sensitivity was achieved by combining automated flux chambers and laser spectroscopy with preconcentration
- We report on the first quasi-continuous analysis of the intramolecular  $^{15}\text{N}$  distribution (known as *site preference*, *SP*) of soil-emitted  $\text{N}_2\text{O}$  over a 3 months period
- Measurements and biogeochemical modeling revealed that denitrification was the dominant  $\text{N}_2\text{O}$  production pathway in the managed grassland

### Supporting Information:

- Supporting Information S1

### Correspondence to:

E. Ibraim,  
erkan.ibraim@usys.ethz.ch







### Citation:

Ibraim, E., Denk, T., Wolf, B., Barthel, M., Gasche, R., Wanek, W., et al. (2020). Denitrification is the main nitrous oxide source process in grassland soils according to quasi-continuous isotopocule analysis and biogeochemical modeling. *Global Biogeochemical Cycles*, 33, e2019GB006505. <https://doi.org/10.1029/2019GB006505>

Received 17 DEC 2019

Accepted 9 MAY 2020

## Denitrification Is the Main Nitrous Oxide Source Process in Grassland Soils According to Quasi-Continuous Isotopocule Analysis and Biogeochemical Modeling

Erkan Ibraim<sup>1,2,6</sup> , Tobias Denk<sup>3</sup>, Benjamin Wolf<sup>3</sup> , Matti Barthel<sup>2</sup>, Rainer Gasche<sup>3</sup> , Wolfgang Wanek<sup>4</sup>, Shasha Zhang<sup>4</sup>, Ralf Kiese<sup>3</sup>, Klaus Butterbach-Bahl<sup>3</sup> , Sarah Eggleston<sup>5</sup>, Lukas Emmenegger<sup>1</sup> , Johan Six<sup>2</sup>, and Joachim Mohn<sup>1</sup> 

<sup>1</sup>Empa, Swiss Federal Laboratories for Materials Science and Technology, Laboratory for Air Pollution and Environmental Technology, Dübendorf, Switzerland, <sup>2</sup>Department of Environmental Systems Science, ETH-Zürich, Swiss Federal Institute of Technology, Zürich, Switzerland, <sup>3</sup>Institute of Meteorology and Climate Research (IMK-IFU), Karlsruhe Institute of Technology, Garmisch-Partenkirchen, Germany, <sup>4</sup>Department of Microbiology and Ecosystem Science, Division of Terrestrial Ecosystem Research, University of Vienna, Vienna, Austria, <sup>5</sup>PAGES International Project Office, University of Bern, Bern, Switzerland, <sup>6</sup>Now at Department of Environmental Systems Science, ETH-Zürich, Swiss Federal Institute of Technology, Zürich, Switzerland

**Abstract** Isotopic composition of soil-emitted nitrous oxide ( $\text{N}_2\text{O}$ ), especially the intramolecular distribution of  $^{15}\text{N}$  in  $\text{N}_2\text{O}$  known as site preference (SP), can be used to track the two major  $\text{N}_2\text{O}$  emitting soil-processes nitrification and denitrification. Online analysis of SP in ambient air has been achieved recently, yet those approaches only allowed addressing large areas (footprints) on the basis of strong changes in surface atmospheric  $\text{N}_2\text{O}$  concentrations. Here, we combined laser spectroscopy with automated static flux chambers to measure, for the first time, SP of low  $\text{N}_2\text{O}$  fluxes with high sensitivity and temporal resolution and to explore its spatial variability. The measurements were then used to test the  $\text{N}_2\text{O}$  isotope module SIMONE in combination with the biogeochemical model LandscapeDNDC to identify  $\text{N}_2\text{O}$  source processes. End-member mixing analysis of the data revealed denitrification as the predominant  $\text{N}_2\text{O}$  source. This finding was independent of the soil water content close to the soil surface, suggesting that  $\text{N}_2\text{O}$  production in the subsoil under high water-filled pore space conditions outweighed the potential production of  $\text{N}_2\text{O}$  by nitrification closer to the surface. Applying the SIMONE-LandscapeDNDC model framework to our field site showed that the modeled SP was on average 4.2‰ lower than the observed values. This indicates that the model parameterization reflects the dominant  $\text{N}_2\text{O}$  production pathways but overestimates the contribution of denitrification by 6%. Applying the stable isotope-based model framework at other sites and comparing with other models will help identifying model shortcomings and improve our capability to support  $\text{N}_2\text{O}$  mitigation from agricultural ecosystems.

**Plain Language Summary** Between August and December 2017 the concentration and isotopic composition of soil emitted nitrous oxide ( $\text{N}_2\text{O}$ ) was measured above a grassland site in Central Switzerland. Automated flux chambers were coupled to a custom-built preconcentration and laser spectroscopy-based online measurement method. The obtained results were used to validate a recently developed isotope submodule (SIMONE) for a biogeochemical model (LandscapeDNDC), to simulate fluxes of trace gases. Our results show a clear predominance of denitrification as the primary  $\text{N}_2\text{O}$  emitting source process. In contrast to previous studies, this dominance led to stable  $\text{N}_2\text{O}$  site preference values throughout the measurement campaign, a feature that was also represented by SIMONE. These findings will bridge current shortcomings in our model understanding and thereby help developing targeted  $\text{N}_2\text{O}$  mitigation strategies.

## 1. Introduction

Nitrous oxide ( $\text{N}_2\text{O}$ ) is a potent greenhouse gas (GHG) and accounts for 6% of the total anthropogenic radiative forcing (Ravishankara et al., 2009). Furthermore, it is the main stratospheric ozone ( $\text{O}_3$ ) depleting

substance. The mean tropospheric abundance of N<sub>2</sub>O has steadily increased from  $270 \pm 7$  ppb (IPCC, 2013) during the preindustrial era to  $328.9 \pm 0.1$  ppb in 2016 (WMO & GAW, 2017) at an average rate of  $0.73 \pm 0.03$  ppb year<sup>-1</sup> over the last three decades (IPCC, 2013). The main driver behind the observed increase of atmospheric N<sub>2</sub>O is the use of fertilizer in agriculture, which fuels microbial N<sub>2</sub>O production in soils (IPCC, 2013). N<sub>2</sub>O emissions from soils are closely linked to the microbial processes nitrification, during which NH<sub>4</sub><sup>+</sup> is oxidized to NO<sub>3</sub><sup>-</sup>, and denitrification, a process during which NO<sub>3</sub><sup>-</sup> is reduced to N<sub>2</sub>. As any biological process, nitrification and denitrification depend on environmental conditions, which are known to vary significantly on small spatiotemporal scales. However, understanding how much of the two processes finally drives soil N<sub>2</sub>O emissions is essential for developing targeted N<sub>2</sub>O mitigation strategies. Although source attribution on sectorial level, that is, to categories like agriculture, industry, or biomass burning, is possible (Davidson & Kanter, 2014), the partitioning of soil N<sub>2</sub>O emissions to the underlying processes (source partitioning) remains challenging, for instance, because different N<sub>2</sub>O producing processes do occur simultaneously.

More recently, the intramolecular isotopic composition of soil emitted N<sub>2</sub>O has been identified to be a powerful tool for disentangling source processes (Decock & Six, 2013; Sutka et al., 2006; Toyoda et al., 2005). The relative abundance of the four most abundant singly substituted N<sub>2</sub>O isotopocules, <sup>14</sup>N<sup>14</sup>N<sup>16</sup>O (99.03%), <sup>14</sup>N<sup>15</sup>N<sup>16</sup>O (0.36%), <sup>15</sup>N<sup>14</sup>N<sup>16</sup>O (0.36%), and <sup>14</sup>N<sup>14</sup>N<sup>18</sup>O (0.20%), is expressed with respect to a standard reference material using the delta (δ) notation in permil (‰) according to equation Equation 1.

$$\delta X = (R_{\text{sample}} - R_{\text{standard}}) / R_{\text{standard}} \quad (1)$$

In Equation 1, *X* denotes <sup>15</sup>N<sup>α</sup>, <sup>15</sup>N<sup>β</sup>, or <sup>18</sup>O, while *R* refers to the sample gas or standard gas isotope ratios <sup>14</sup>N<sup>15</sup>N<sup>16</sup>O/<sup>14</sup>N<sup>14</sup>N<sup>16</sup>O (for <sup>15</sup>N<sup>α</sup>), <sup>15</sup>N<sup>14</sup>N<sup>16</sup>O/<sup>14</sup>N<sup>14</sup>N<sup>16</sup>O (for <sup>15</sup>N<sup>β</sup>), or <sup>14</sup>N<sup>14</sup>N<sup>18</sup>O/<sup>14</sup>N<sup>14</sup>N<sup>16</sup>O (for <sup>18</sup>O), respectively (Toyoda & Yoshida, 1999). The <sup>15</sup>N/<sup>14</sup>N ratio is referenced to the international isotope ratio scale atmospheric N<sub>2</sub> (AIR-N<sub>2</sub>), while the <sup>18</sup>O/<sup>16</sup>O ratio is referenced to Vienna Standard Mean Ocean Water (V-SMOW). While the total <sup>15</sup>N content of N<sub>2</sub>O is reported as bulk <sup>15</sup>N content (δ<sup>15</sup>N<sup>bulk</sup>, Equation 2), the predominance for <sup>15</sup>N substitution in the central position is reported as site preference (SP; Equation 3) (Mohn et al., 2016; Toyoda & Yoshida, 1999).

$$\delta^{15}\text{N}^{\text{bulk}} = (\delta^{15}\text{N}^{\alpha} + \delta^{15}\text{N}^{\beta}) / 2, \quad (2)$$

$$\text{SP} = \delta^{15}\text{N}^{\alpha} - \delta^{15}\text{N}^{\beta}. \quad (3)$$

Source partitioning between the process groups (i) (nitrifier) denitrification (N<sub>2</sub>O<sub>D</sub>) versus (ii) nitrification, abiotic N<sub>2</sub>O production, and fungal denitrification (N<sub>2</sub>O<sub>N</sub>) is possible, as the SP of the emitted N<sub>2</sub>O is distinctly lower for the first (N<sub>2</sub>O<sub>D</sub>,  $-0.9 \pm 4.1\text{‰}$ ) as compared to the second category (N<sub>2</sub>O<sub>N</sub>,  $32.8 \pm 2.2\text{‰}$ ) (Denk et al., 2017; Koba et al., 2009; Lewicka-Szczebak et al., 2017). Generally, two-end-member mixing analysis maps, additionally accounting for isotopic fractionation due to N<sub>2</sub>O reduction by denitrifying bacteria, are applied for data interpretation (Decock & Six, 2013; Ibraim et al., 2019; Koba et al., 2009; Lewicka-Szczebak et al., 2017; Verhoeven et al., 2019; Wolf et al., 2015). This approach has shown potential to source partition in laboratory experiments and in engineered systems under defined reaction conditions or microbial consortia (Koster et al., 2013; Wunderlin et al., 2012), while in natural systems, such unequivocal distinction is impeded. The combination of analytical challenges and the complexity of data interpretation is the reason for the scarcity of studies interpreting N<sub>2</sub>O isotope signatures from natural systems.

For many years, isotope ratio mass spectrometry (IRMS) was the only technique with sufficient sensitivity to trace natural abundances of N<sub>2</sub>O isotopocules (Röckmann et al., 2003; Toyoda & Yoshida, 1999). More recently, laser spectroscopy-based methods were developed and are increasingly used to analyze the stable isotopes of atmospheric trace gases (Süess et al., 2016; Winther et al., 2018). The online analysis of N<sub>2</sub>O isotopocules in ambient air, however, is complicated by the fact that variations in concentration and isotopocule abundances are small (Mohn et al., 2012; Yamamoto et al., 2014). Nevertheless, N<sub>2</sub>O isotopic analysis in ambient air at sensitivities similar to those achieved by IRMS has been presented using a more sophisticated approach deploying quantum cascade laser absorption (QCLAS) spectrometers in combination with automated preconcentration (Harris et al., 2017; Mohn et al., 2010; Wolf et al., 2015). Using a more

compact spectrometer and a more powerful preconcentration device (TRace gas EXtractor, or TREX), the TREX-QCLAS method was recently redesigned by Ibraim et al. (2018) and applied at a grassland site in southern Germany (Ibraim et al., 2019). The measurements reached a level of precision sufficient to resolve changes in ambient  $N_2O$  isotopocule concentrations. Using an end-member mixing analysis approach (Keeling, 1958, 1961), the isotopic composition of soil-emitted  $N_2O$  was determined from  $N_2O$  accumulations in the nocturnal boundary layer. This technique did, however, not allow explicit spatial mapping and could not be implemented during the daytime due to atmospheric mixing. Higher temperatures and evaporation during the day alter the soil environmental conditions, which in turn might favor either  $N_2O_N$  or  $N_2O_D$ . Consequently, short-term changes in the relative contributions of  $N_2O$  produced via  $N_2O_N$  and  $N_2O_D$  due to diurnal variation of soil conditions may be concealed if measurements are restricted to the night.

Biogeochemical models such as DNDC/LandscapeDNDC (Li et al., 1992a, 1992b; Li et al., 2000), CERES (Gabrielle et al., 2006), and DAYCENT (Del Grosso et al., 2000; Parton et al., 2001) simulate relevant N cycling processes and their dependence on soil environmental conditions. These models are increasingly used to assess the fate of N species in the environment, to transfer observations at a specific site to different soils and climates, and to evaluate agricultural management options to reduce the release of  $N_2O$  and other N losses (Kim et al., 2015; Molina-Herrera et al., 2016). The parameterization of biogeochemical models can be improved combining models with the process information contained in the  $N_2O$  isotopic composition. Despite this potential for improvements, the implementation of isotopes in biogeochemical models has lagged behind (Rastetter et al., 2005). First steps in this direction have been made for the CLM-CN model (Houlton et al., 2015), the DAYCENT model (Bai & Houlton, 2009), and the nonequilibrium stable isotope simulator NESIS (Rastetter et al., 2005). Recently, Denk et al. (2019) developed the “Stable Isotope Model for Nutrient cycles” model (SIMONE), which uses fluxes between ecosystem N pools (soil organic N, mineral N, plants, and microbes) calculated by biogeochemical models and literature isotope effects to calculate the isotopic composition of soil N pools and  $N_2O$  emissions.

The objectives of this study were to (i) quantify fluxes (we use the term flux to describe the “emission of gas per unit area per unit time”) and isotopic composition of  $N_2O$  emitted from a grassland site in central Switzerland, (ii) map emissions explicitly in space and time by using flux chambers to repeatedly determine the isotopic composition of  $N_2O$  emitted from soil during the day, (iii) use the obtained data to source partition major soil microbial processes by carrying out end-member mixing model analysis, and (iv) assess the process parameterization of the biogeochemical model LandscapeDNDC by comparing measured fluxes and isotopic signatures of  $N_2O$  with results obtained using the LandscapeDNDC-SIMONE modeling framework.

## 2. Material and Methods

### 2.1. Characterization of the Research Site Beromünster

#### 2.1.1. Study Site

The study site is located on top of a hill at 797 m a.s.l in the vicinity of the decommissioned radio tall tower of Beromünster (BRM; N: 47°11'22", E: 8°10'32") in central Switzerland. BRM was established as a measurement station for GHG monitoring within the SNF Sinergia project CarboCount (Oney et al., 2015) and in 2016 integrated to the Swiss National Air Pollution Monitoring Network (NABEL). In 2017, the mean annual precipitation and temperature were 1,142 mm and 9.1°C, respectively. The experimental site was a 10 m × 30 m area, which is part of a 3-ha grassland west of the tall tower (Figure S1 in the supporting information). The grasslands surrounding the Beromünster tower were grazed by cattle during the study period. Soil properties at the BRM study site are given in Table 1.

As indicated in Figure S1, the study site was subdivided into Sections B1, B2, and BF. Both B1 and B2 were equipped with three automated static chambers that were opened and closed by means of pneumatic actuators to determine  $N_2O$  fluxes during chamber closure. While B1 chambers were exclusively used for  $N_2O$  flux measurements, headspace air from the B2 chambers was preconcentrated for determination of  $N_2O$  isotopic composition. BF represents a 1 m × 1 m section that was treated identically to the B1 and B2 chambers' area regarding fertilizer addition and was used for soil sampling after fertilization in order to keep the ongoing measurements in Sections B1 and B2 undisturbed. When no recent fertilizer application had occurred, biweekly soil sampling was conducted at B1 and B2 (see section 2.1.3).

**Table 1**  
Soil Properties Within the Perimeter of the Experimental Site Beromünster

Depth (cm)	Bulk density ( $\text{g cm}^{-3}$ )	C <sub>org</sub> (%)	N <sub>tot</sub> (%)	pH (a.u.)	Clay (%)	Silt (%)	Sand (%)
7	1.3 ± 0.1	3.5 ± 0.5	0.6 ± 0.3	5.5	24.6 ± 0.5	42.9 ± 0.2	32.5 ± 0.6
14	1.4 ± 0.0	1.8 ± 0.2	0.2 ± 0.0	5.3	22.9 ± 0.4	40.1 ± 1.5	37.0 ± 1.4
32	1.4 ± 0.1	0.9 ± 0.3	0.1 ± 0.0	5.5	25.8 ± 1.4	39.2 ± 2.0	35.0 ± 1.2
50	1.5 ± 0.1	0.5 ± 0.1	0.1 ± 0.0	5.6	26.9 ± 0.5	40.6 ± 0.7	32.5 ± 1.1

### 2.1.2. Environmental Conditions and Agricultural Management

A wide range of meteorological and air quality-related data are available from 15 March 2017 onward, including air temperature and precipitation. In addition, a soil temperature profile (depths of 5, 10, and 15 cm) was installed between Sites B1 and B2 using three PT100 sensors (IMKO, Ettlingen, Germany), and soil temperature in 5 cm depth was measured at B1 and B2 using the same type of sensors. A precipitation sensor (Campbell ARG100, Campbell Scientific, USA) was used to open the chambers upon rainfall. Soil volumetric water content (VWC) was determined with four ThetaML2x probes (Delta-T Devices, Cambridge, UK) distributed across the experimental site. While the probes integrate the VWC over a soil depth of 0–6 cm, water-filled pore space (WFPS) was calculated according to measured VWC by taking into account the observed soil characteristics (Wu et al., 2010).

Agricultural management comprised mowing (17 May, 19 June, 29 August, and 24 October 2017) and fertilization. While the surrounding grassland site received two loads of manure on 27 May and 18 November, the perimeter of the experimental site was not manured to avoid cross-interference with own fertilizer-addition experiments.

### 2.1.3. N<sub>2</sub>O Fluxes, Concentration of Soil Extracted NH<sub>4</sub><sup>+</sup> and NO<sub>3</sub><sup>−</sup>, and $\delta^{15}\text{N}$ of NH<sub>4</sub><sup>+</sup> and NO<sub>3</sub><sup>−</sup>

Two sets of three chamber frames were inserted into the soil for each of the blocks (B1 and B2) a week before the measurements began. Adverse effects on the vegetation arising from shadowing were minimized by regularly mounting the chambers to the alternative frames. Fluxes of soil-emitted N<sub>2</sub>O ( $f_{\text{N}_2\text{O}}$ ) were measured between 23 August and 1 December 2017 using three opaque static chambers (hereafter referred to as “chambers”; 0.5 × 0.5 × 0.5 m) in combination with a field-deployable gas chromatograph with an electron capture detector (GC-ECD, GC-17A, Shimadzu) contained in a trailer. The chambers automatically closed for 48 min during which each chamber was consecutively sampled for 3 min. At the end of the 3 min period, 3 ml air was automatically injected into the GC-ECD for determination of N<sub>2</sub>O mixing ratio, yielding four N<sub>2</sub>O concentration measurements per chamber and closure cycle. In addition, calibration gas was injected twice every 24 min. Between flux measurements, the three chambers remained open for 48 min. Fluxes were calculated based on the increase of N<sub>2</sub>O mixing ratios. Details of the method were previously presented by Butterbach-Bahl et al. (1997) and Rosenkranz et al. (2006).

Soil samples were collected biweekly between 23 August and 29 November, with increased sampling frequency during the fertilization experiments. In total, 116 soil samples of approximately 150 g (0–6 cm depth) were taken from the surroundings of the flux chambers (prior to the fertilizer addition experiments) and from the section BF (during the fertilizer addition experiments as described in section 2.4). Soil (100 g) was extracted with 150 ml 1 M potassium chloride (KCl, Merck KGaA, Germany), filtered (GE Healthcare Life Sciences, Whatman GF/A, United Kingdom), and the soil extracts were stored at −20°C. Subsequently, NH<sub>4</sub><sup>+</sup> and NO<sub>3</sub><sup>−</sup> concentrations were determined colorimetrically with a spectrophotometer (AGROLAB Agrarzentrum GmbH, Germany).

In addition, all soil extracts were analyzed for  $\delta^{15}\text{N}$ -NO<sub>3</sub><sup>−</sup> and  $\delta^{15}\text{N}$ -NH<sub>4</sub><sup>+</sup> using chemical methods (Lachouani et al., 2010; Zhang et al., 2015).  $\delta^{15}\text{N}$ -NH<sub>4</sub><sup>+</sup> signatures were determined with the same method as  $\delta^{15}\text{N}$ -NO<sub>3</sub><sup>−</sup> signatures after microdiffusion of NH<sub>4</sub><sup>+</sup> and alkaline persulfate oxidation of NH<sub>4</sub><sup>+</sup> to NO<sub>3</sub><sup>−</sup>. NO<sub>3</sub><sup>−</sup> was subsequently converted via NO<sub>2</sub><sup>−</sup> to N<sub>2</sub>O by acidic VCl<sub>3</sub> reduction and sodium azide reaction (Lachouani et al., 2010). Isotopic composition of N<sub>2</sub>O was then measured by purge-and-trap isotope ratio mass spectrometry (cryotrap Gasbench - Delta V Advantage, Thermo Fisher, Vienna, Austria) and calibrated using appropriate natural <sup>15</sup>N abundance standards (Lachouani et al., 2010). The standard deviation of repeated measurements of a reference material was <0.2‰. The analytical work was carried out between



12 February and 2 March 2018 in the SILVER stable isotope laboratory at the Division of Terrestrial Ecosystem Research, University of Vienna.

#### 2.1.4. N<sub>2</sub>O Isotopocule Analysis

Between 29 August and 4 December, 610 and 828 measurements were obtained from the 2 m inlet and from the headspaces of the three B2 chambers, respectively, all being analyzed with the TREX-QCLAS for concentration and isotopic composition of N<sub>2</sub>O (Figure S2). A pressurized air tank (T) with an N<sub>2</sub>O concentration and isotopic composition similar to that of ambient air was measured 542 times along with the ambient air measurements (Figures S3–S6). According to those 542 T measurements, the long-term analytical repeatability of the measurements spanning the whole measurement period was 0.61‰, 0.55‰, 0.47‰, and 3.3 ppb for  $\delta^{15}\text{N}^{\alpha}$ ,  $\delta^{15}\text{N}^{\beta}$ ,  $\delta^{18}\text{O}$ , and N<sub>2</sub>O concentration measurements, respectively. The accuracy of the applied technique was additionally assessed by triplicate in situ measurements of T, T1, and T2 undergoing identical treatment as the sample measurements by TREX-QCLAS and IRMS at ETH and at the Tokyo Institute of Technology (Tokyo Tech; Figure S7 and Tables S1 and S2). Average deviations of TREX-QCLAS to IRMS measurements are in the range 0.21–0.35‰ (IRMS ETH) and 0.03–0.48‰ (IRMS Tokyo Tech) for all isotope deltas ( $\delta^{15}\text{N}^{\alpha}$ ,  $\delta^{15}\text{N}^{\beta}$  and  $\delta^{18}\text{O}$ ), indicating an excellent degree of accuracy.

#### 2.1.5. N<sub>2</sub>O Isotopocule Analysis With IRMS

For an independent validation, the target gases T, T1, and T2 as well as the sample gases from the chamber headspace of 26 September were analyzed with IRMS at the Department of Environmental Systems Science, ETH Zurich (Verhoeven et al., 2019). To this end, discrete air samples were collected from the chamber headspace through a sample port using a 60 ml syringe at 0, 20, 40, 60, 80, 110, and 130 min time intervals after chamber closure. Subsamples from each time point were immediately injected in pre-evacuated 12 ml Labco exetainer and 110 ml serum crimp vials for GC (456-GC, Scion Instruments, Livingston, UK) and IRMS (IsoPrime100, Elementar, UK) analysis, respectively. Sampling was conducted for all three chambers, leading to a total of 21 samples. Sampling from tank T, T1, and T2 was done in a similar fashion, using a sampling port at the pressure valve (Table S1).

## 2.2. N Addition Experiments

To investigate the response of the N<sub>2</sub>O isotopic composition to changes in substrate availability and environmental conditions, a set of experiments was designed aiming to trigger (i) nitrification and (ii) complete denitrification (i.e., N<sub>2</sub>O reduction). For this purpose, 70 kg N ha<sup>−1</sup>, either in the form of ammonium sulfate ((NH<sub>4</sub>)<sub>2</sub>SO<sub>4</sub>, ≥99% purity, Sigma-Aldrich Chemie GmbH, Switzerland) or potassium nitrate (KNO<sub>3</sub>, ≥99% purity, Sigma-Aldrich Chemie GmbH, Switzerland) was added following the procedure described below. As shadowing effects were negligible in November, only one frame set, that is, three frames, of both B1 and B2 was supplied with fertilizer. This approach had the advantage that we could compare the fertilized plots with nonfertilized plots. Hereafter, the framesets that have received fertilizer will be referred to as *treatment* framesets, while the framesets that have not received fertilizer will be referred to as *reference* framesets. After the fertilizer addition, the position of the B2 chambers was alternated daily between the treatment and reference frameset to test effects caused by the fertilizer addition. At B1, chambers remained on the treatment frameset. Details on the fertilizer addition can be found in the supporting information.

As mentioned in sections 2.1.1 and 2.1.2, typical management practices at BRM include cattle grazing, manure application, and mowing. Within the presented NH<sub>4</sub><sup>+</sup> and NO<sub>3</sub><sup>−</sup> application treatments, we used mineral fertilizers to stimulate specific microbial pathways, partly at the expense of representing typical grassland management practices. At the same time, the presented approach is a clear step forward in source partitioning N<sub>2</sub>O fluxes to microbial processes within the framework of an open grassland ecosystem.

#### 2.2.1. Isotopic Characterization of Fertilizers

The fertilizers ((NH<sub>4</sub>)<sub>2</sub>SO<sub>4</sub> and KNO<sub>3</sub>) were analyzed for their  $\delta^{15}\text{N}$  signature at the Department for Environmental Systems Science, ETH Zurich, using IRMS. The instrumentation consisted of an elemental analyzer (Flash EA, Thermo Fisher Scientific, MA, USA) coupled to a Delta<sup>plus</sup>XP Isotope Ratio Mass Spectrometer with a six-port valve and a ConFlo III interface (Finnigan MAT, HB, Germany). Details of this method are presented by Werner et al. (1999). Obtained  $\delta^{15}\text{N}^{\text{bulk}}$  values of (NH<sub>4</sub>)<sub>2</sub>SO<sub>4</sub> and KNO<sub>3</sub> corresponded to  $16.11 \pm 0.04\text{‰}$  and  $3.25 \pm 0.01\text{‰}$ , respectively.

### 2.3. Keeling Plot Analysis and Daily Mean Source Signatures

Source signatures of soil-emitted  $\text{N}_2\text{O}$  were derived using the Keeling plot approach (Keeling, 1958, 1961). The measurement routine allowed for one Keeling plot analysis for each B2 chamber per day. Retrieved signatures were only interpreted further if the Keeling plots' linear model was statistically significant, which was the case in 264 of 276 Keeling plots. To account for spatial heterogeneity, the source signatures derived for the three chambers were then pooled into daily mean values, weighing signatures of individual chamber measurements with the observed  $\text{N}_2\text{O}$  fluxes.  $\delta^{15}\text{N}^{\text{bulk}}$  signatures of  $\text{N}_2\text{O}$  prior to fertilizer application were corrected for the substrate  $\delta^{15}\text{N}^{\text{bulk}}\text{-NO}_3^-$  and  $\delta^{15}\text{N}^{\text{bulk}}\text{-NH}_4^+$  values as suggested by Koba et al. (2009), while for the period after the fertilizer addition also, the  $\delta^{15}\text{N}^{\text{bulk}}$  values of applied  $(\text{NH}_4)_2\text{SO}_4$  or  $\text{KNO}_3$  were used. Statistical analysis was carried out using Matlab (MathWorks, Inc., MA, USA), and  $p < 0.05$  was chosen as significance threshold unless stated otherwise.

### 2.4. Biogeochemical and Isotope Modeling Using LandscapeDNDC and SIMONE

LandscapeDNDC (Grote et al., 2009; Haas et al., 2013) is a biogeochemical model simulation framework for terrestrial ecosystems to simulate carbon (C) and N cycling in agricultural and forest ecosystems (Kim et al., 2015; Kraus et al., 2015; Molina-Herrera et al., 2015). In this study, biogeochemistry, soil hydrology, and vegetation growth were modeled using the modules DNDC, WatercycleDNDC (Kiese et al., 2011), and GrasslandDNDC (Li et al., 2000; Molina-Herrera et al., 2016), respectively. The model setup requires input data on precipitation, temperature, vegetation, soil characteristics, and agricultural management. Soil characteristics comprise depth profiles of soil texture, soil organic carbon, total nitrogen, bulk density, and soil hydraulic properties. In this study, the soil profile was divided into 40 layers. Layers in the topsoil and subsoil were 1 and 1.8 cm thick, respectively.

The Stable Isotope MOdel for Nutrient cycles (SIMONE; Denk et al., 2019) calculates the isotopic composition of the N pools simulated by a parent biogeochemical model (here LandscapeDNDC). To this end, SIMONE uses the pool sizes and fluxes from a given simulation to calculate the isotopic composition of soil N pools such as  $\text{NH}_4^+$ ,  $\text{NO}_3^-$ , and  $\text{N}_2\text{O}$ . This is based on the fraction of substrate converted to the product and the corresponding isotope fractionation factor of each transformation process (Denk et al., 2017) and applies the closed-system Rayleigh isotope fractionation equations (Mariotti et al., 1981). SIMONE follows the sequence of the process calculations dictated by the parent model; that is, the cumulative product of a preceding reaction becomes the initial product of the following reaction in the sequence. The SIMONE model was previously presented in detail by (Denk et al., 2019), while a brief description can also be found in Figure S10.

## 3. Results

### 3.1. Environmental Conditions and Rates of Soil Emitted $\text{N}_2\text{O}$

Between 23 and 28 August 2017 the ambient air temperature was between 14.5°C and 24.9°C, and since only little precipitation occurred during that period, the water filled pore space (WFPS) steadily decreased from approximately 70% to 50%. The experimental site was mown on 29 August. Between 31 August and 3 September, continuing rainfall of around 15 mm day<sup>-1</sup> was observed, driving WFPS to values beyond 90% (Figure 1). At the same time, the soil temperature dropped by approximately 7°C. Thereafter, the rainfall ceased while the temperatures steadily increased again.

Between 6 November and 1 December, which corresponds to the period of the fertilizer addition experiments, ambient and soil temperatures steadily decreased reaching soil temperatures close to 0°C at 5 cm depth. On 6 November, in parallel with the initialization of the fertilizer addition experiments, the first snowfall of the season was observed at BRM.

The  $\text{NH}_4^+$  concentrations prior to the fertilizer addition, that is, between 23 August and 5 November, were  $3.5 \pm 0.9$  and  $4.6 \pm 1.0$   $\mu\text{g NH}_4^+ \text{ g}^{-1}$  soil at B1 and B2, respectively. The  $\text{NO}_3^-$  concentrations during the same time were  $5.2 \pm 2.9$  and  $3.3 \pm 1.7$   $\mu\text{g NO}_3^- \text{ g}^{-1}$  soil at B1 and B2, respectively (Figures 1g and S8). While  $\text{NO}_3^-$  concentrations did not systematically change from August to October,  $\text{NH}_4^+$  values showed a slight positive trend, reaching values of 5.1 and 6.6  $\mu\text{g NH}_4^+ \text{ g}^{-1}$  soil at B1 and B2 by 17 October.  $\text{NH}_4^+$  fertilization on 6

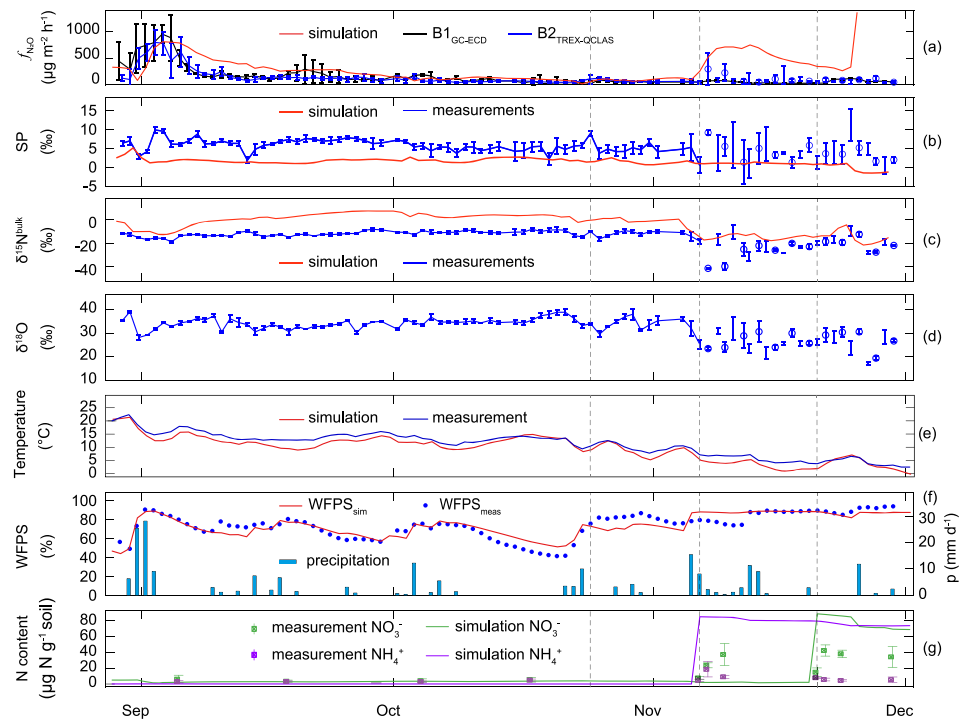


**Figure 1.** (a)  $N_2O$  fluxes obtained by measurements with GC-ECD and TREX-QCLAS at Sections B1 and B2 of the experimental site and by simulation with SIMONE. Error bars indicate observed variation ( $1\sigma$ ). (b), (c), and (d) depict the observed and simulated source signatures SP,  $\delta^{15}N^{bulk}$ , and  $\delta^{18}O$ , where consigned circles after 6 November indicate measurements from chamber frames that received fertilizer, while absence of circles refers to reference frameset measurements (no fertilizer received). Indicated error bars refer to  $1\sigma$  variation according to a Monte Carlo simulation ( $n = 200$ ) in (b) and to  $1\sigma$  variation of obtained data in (c) and (d). (e) Observed and simulated soil temperature at 5 cm soil depth. (f) Observed and simulated water filled pore space (WFPS) and observed precipitation. (g) Measured (squares with  $1\sigma$  variation error bars) and simulated  $NH_4^+$  and  $NO_3^-$  concentrations in  $\mu g\ g^{-1}$  soil. Dashed vertical lines indicate mowing of the experimental site (24 October) and addition of  $70\ kg\ N\ ha^{-1}$  ( $(NH_4)_2SO_4$  and  $KNO_3$  on 6 November and 20 November 2017, respectively).

November led to an increase of both  $NH_4^+$  and  $NO_3^-$  concentrations, while  $NO_3^-$  fertilization led to increased  $NO_3^-$  concentrations only.

$N_2O$  fluxes were highest between 29 August and 7 September on both sections (B1 and B2) of the experimental site with peak emission rates between  $500$  and  $1,000\ \mu g\ N_2O\ m^{-2}\ h^{-1}$  (Figure 1a). After 12 September, the  $N_2O$  fluxes were relatively stable and resulted in an average rate of  $120 \pm 50\ \mu g\ N_2O\ m^{-2}\ h^{-1}$ . Fluxes higher than  $500\ \mu g\ N_2O\ m^{-2}\ h^{-1}$  were associated with soil temperatures greater than  $20^\circ C$  and WFPS values of 80% to 95% (Figure 3).  $N_2O$  emission rates slightly increased in the B2 treatment frameset immediately after the mineral fertilizer ( $NH_4^+$ ) addition on 6 November. After the  $NO_3^-$  addition on 20 November, no increase of the  $N_2O$  fluxes was observed.

### 3.2. Source Signatures of Soil-Emitted $N_2O$

The  $\delta^{15}N^\alpha$ ,  $\delta^{15}N^\beta$ , and  $\delta^{18}O$  values obtained from open chambers, thus representing atmospheric background values, were  $15.45 \pm 0.82\text{‰}$ ,  $-3.07 \pm 0.59\text{‰}$ , and  $44.69 \pm 0.52\text{‰}$ , respectively. In the period before fertilizer addition, the daily mean SP,  $\delta^{15}N^{bulk}$ , and  $\delta^{18}O$  values of soil-emitted  $N_2O$ , that is, the flux weighed Keeling plot derived source signatures, were  $5.8 \pm 1.6\text{‰}$ ,  $-11.8 \pm 2.3\text{‰}$ , and  $34.8 \pm 2.3\text{‰}$ , respectively (Figures 1b–1d). The  $(NH_4)_2SO_4$  addition on 6 November caused a decrease in mean SP,  $\delta^{15}N^{bulk}$ , and  $\delta^{18}O$  values of  $N_2O$ , leading to  $4.5 \pm 2.8\text{‰}$ ,  $-28.1 \pm 8.6\text{‰}$ , and  $30.5 \pm 4.3\text{‰}$ , respectively. Finally, after the  $KNO_3$  addition on 20 November mean SP,  $\delta^{15}N^{bulk}$ , and  $\delta^{18}O$  values resulted in  $3.1 \pm 1.4\text{‰}$ ,  $-20.0 \pm 5.5\text{‰}$ , and  $35.0 \pm 4.4\text{‰}$ , respectively.

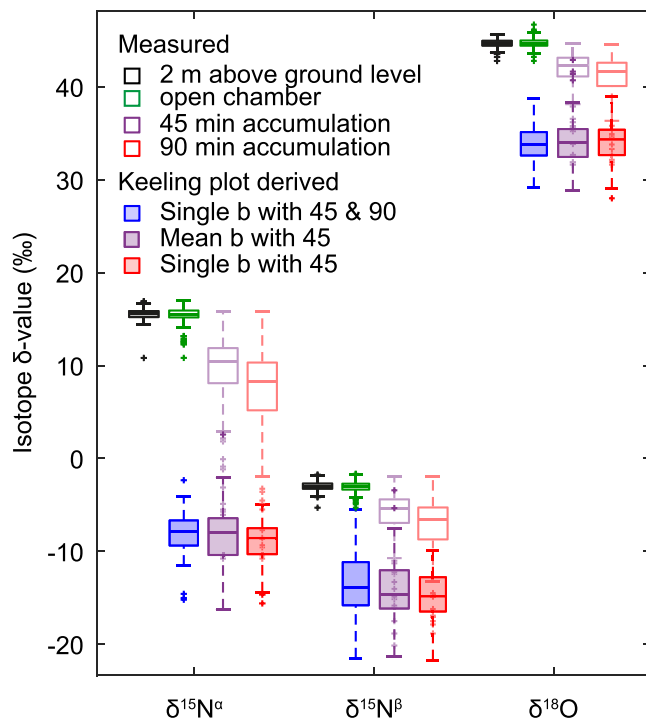


**Figure 2.** Variability of  $\delta^{15}\text{N}^\alpha$ ,  $\delta^{15}\text{N}^\beta$ , and  $\delta^{18}\text{O}$  values in background air at daytime (green), after 45 min chamber closure (empty pale purple boxplots) and after 90 min chamber closure (empty pale red boxplots). Black boxplots represent the isotope  $\delta$  values obtained at night from the 2 m above ground level sample inlet. Filled boxplots illustrate Keeling plot-derived isotope  $\delta$  values as obtained from individual background (i.e., open chamber) measurements in conjunction with 45 and 90 min chamber closure measurements (blue), daily mean background measurements in conjunction with 45 min chamber closure (purple), and individual background measurements in conjunction with 45 min chamber closure measurements (red).

( $3.5 \mu\text{g g soil}^{-1}$ ), while  $\text{NO}_3^-$  concentrations were also underestimated, but to a lower degree, with  $2.8 \mu\text{g g soil}^{-1}$  (simulated) and  $5.2 \mu\text{g g soil}^{-1}$  (measured), respectively.

### 3.3.1. Isotope Modeling

Based on the LandscapeDNDC output, SIMONE was used to calculate  $\delta^{15}\text{N}^{\text{bulk}}$  and SP. While simulated  $\delta^{15}\text{N}^{\text{bulk}}$  values were higher compared to the measurements (RMSE of 12.3‰), the low variability of  $\delta^{15}\text{N}^{\text{bulk}}$  before fertilizer addition agreed well with the measurements. After ammonium fertilization, the depletion of  $\delta^{15}\text{N}^{\text{bulk}}$  was lower in the LandscapeDNDC-SIMONE simulations as compared to the measurements, which, however, showed a large variability. In contrast, for the  $\text{KNO}_3$  fertilization, simulated and measured  $\delta^{15}\text{N}^{\text{bulk}}$  agreed well, and the decline in soil  $\text{NO}_3^-$  concentration following peak concentrations immediately after  $\text{KNO}_3$  application coincided with a decline in  $\delta^{15}\text{N}^{\text{bulk}}$  (Figure 1c). With regard to SP, the LandscapeDNDC-SIMONE simulations produced lower values as compared to measurements throughout the campaign, only showing a slight increase in SP of approximately 3‰ on 31 August. While the observations showed slightly larger variability throughout the measurement campaign, the simulated SP values were very stable at  $1.43 \pm 0.96\text{‰}$  (Figure 1b).

## 4. Discussion

### 4.1. Methodological Considerations

To determine the isotopic composition of  $\text{N}_2\text{O}$  emitted from soils in situ, previous studies have relied on Keeling plots (Ibraim et al., 2019; Wolf et al., 2015). This approach presumes mixing of the atmospheric background with soil air at a higher  $\text{N}_2\text{O}$  concentration and, thus, a change of  $\text{N}_2\text{O}$  concentration. For this

The TREX-QCLAS-derived measurements were cross-validated on 26 September by parallel GC/IRMS measurements and Keeling plot analysis. Source signatures determined by GC/IRMS of  $4.94 \pm 2.69\text{‰}$ ,  $-10.64 \pm 2.96\text{‰}$ , and  $29.31 \pm 3.01\text{‰}$  for SP,  $\delta^{15}\text{N}^{\text{bulk}}$ , and  $\delta^{18}\text{O}$  (mean  $\pm 1$  SD,  $n = 3$  chambers) agreed with TREX-QCLAS results of  $7.54 \pm 1.60\text{‰}$ ,  $-11.70 \pm 4.62\text{‰}$ , and  $30.06 \pm 3.24\text{‰}$  (SP,  $\delta^{15}\text{N}^{\text{bulk}}$ , and  $\delta^{18}\text{O}$ ) within one standard deviation.

### 3.2.1. Correlation of $\delta^{18}\text{O}\text{-N}_2\text{O}$ With WFPS

During the campaign, WFPS ranged from 40% to 90%. Over this WFPS range,  $\delta^{18}\text{O}\text{-N}_2\text{O}$  decreased from approximately 45‰ to 25‰ and showed a significant negative correlation to WFPS ( $p < 0.001$ ). The relationship of the  $\delta^{18}\text{O}$  values in dependence of the WFPS values was best explained with the exponential model  $y = -5.51\text{e-}10 \times \exp(0.24 \times \text{WFPS}) + 50.84 \times \exp(-2.91\text{e-}03 \times \text{WFPS})$  shown in Figure 3.

### 3.3. Biogeochemical Modeling

Soil environmental conditions simulated by LandscapeDNDC agreed well with the measured conditions (Figures 1e and 1f). For soil water content, this is reflected by the high coefficient of correlation ( $R$ ) of 0.86 and the low root mean square error (RMSE) of 6.7% (average simulated = 76.2%, measured = 75.2% from 29 August to 30 November 2017). The high  $R$  and low RMSE of soil temperature (0.97 and 1.92 K, respectively) indicate a good representation of soil temperature dynamics and accuracy. With moderate baseline emissions of 60 to  $150 \mu\text{g N}_2\text{O m}^{-2} \text{hr}^{-1}$ , one major (beginning of September) and two minor emission events (mid-September and mid-October), the measured and simulated  $\text{N}_2\text{O}$  emissions showed the same features. However, timing of the simulated, rainfall-induced  $\text{N}_2\text{O}$  emission peaks was biased as well as the decline in emissions following the peak emission periods. This as well as the too high baseline emission rates at the beginning of the measurements resulted in  $R$  and high RMSE values of 0.51 and  $260 \mu\text{g N}_2\text{O m}^{-2} \text{hr}^{-1}$ , respectively. Prior to fertilizer addition, simulated soil  $\text{NH}_4^+$  concentrations ( $0.11 \mu\text{g g soil}^{-1}$ ) were lower than the measured concentrations



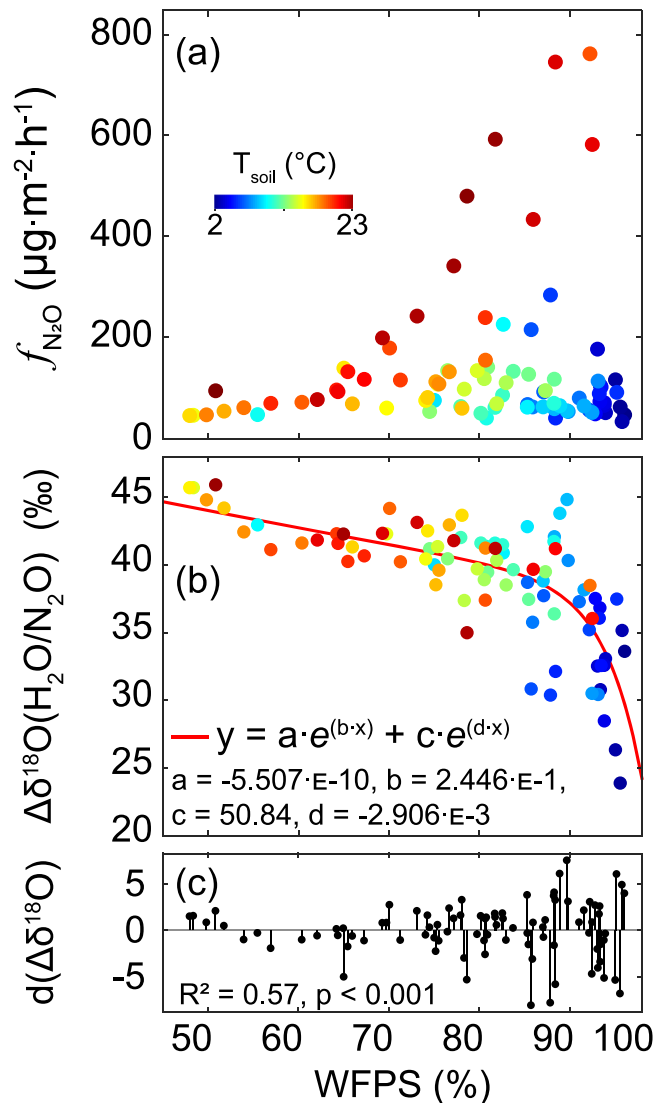


**Figure 3.** (a) Observed daily mean  $\text{N}_2\text{O}$  fluxes versus water filled pore space (WFPS), (b)  $\Delta\delta^{18}\text{O}\text{-N}_2\text{O}$  versus WFPS and the related nonlinear fit (red curve) with the given model parameters, and (c) deviations of observed  $\Delta\delta^{18}\text{O}$  values from the derived function. In (a) and (b) the color code refers to the corresponding soil temperature according to the legend given in (a).

individual/mean background air measurements. Due to the excellent signal-to-noise ratios, none of the investigated scenarios was statistically different (Figure 2). Therefore, the measurement frequency can be substantially increased in future studies by carrying out the Keeling plot analysis based on one single background measurement per day combined with individual analyses 45 min after chamber closure. With this adaptation, a frequency of approximately one source signature measurement per hour will be achieved, which is a clear step forward in monitoring and understanding short-term dynamics of the soil processes involved in  $\text{N}_2\text{O}$  emissions.

#### 4.2. Environmental Controls on $\text{N}_2\text{O}$ Fluxes and Isotope Signatures

Between end of August and end of September,  $\text{N}_2\text{O}$  emission rates obtained at BRM were comparable to those found in previous grassland related studies in Switzerland and Germany (Hörtnagl et al., 2018; Ibraim et al., 2019; Merbold et al., 2014; Wolf et al., 2015). As also observed previously,  $\text{N}_2\text{O}$  emission rates significantly correlated with WFPS values at BRM (Figure 3), with a positive correlation between 40% and

reason, the named studies used measurements taken at overnight periods since  $\text{N}_2\text{O}$  concentration increases in the nocturnal boundary layer due to a decrease of the mixing layer height under stable atmospheric conditions. A major constraint of this approach is the fact that  $\text{N}_2\text{O}$  accumulation in the NBL hardly results in  $\text{N}_2\text{O}$  concentrations beyond 400 ppb, while at most of the night hours, maximum  $\text{N}_2\text{O}$  concentrations of 350 ppb could be observed. Furthermore, a stable NBL is only present if advantageous conditions regarding meteorology and topography are provided (Garratt, 1994); otherwise, no  $\text{N}_2\text{O}$  concentration increase may be observed, obviating Keeling plot analysis of the isotope signatures of soil  $\text{N}_2\text{O}$ . Therefore, in a recent study out of 30 days of measurements comprising close to 600 individual measurements, only 12 Keeling plot-derived source signatures could be retrieved (Ibraim et al., 2019).

Within the present study, for the first time a combined approach of automated flux chambers and TREX-QCLAS was achieved. Accumulating soil-emitted  $\text{N}_2\text{O}$  in the chamber headspaces allowed determination of  $\text{N}_2\text{O}$  isotopic composition even at day time. Obtained  $\text{N}_2\text{O}$  isotope  $\delta$  values were lower by 4–9‰ compared to background  $\text{N}_2\text{O}$  isotope  $\delta$  values, thus a factor of 10–20 higher than the analytical precision of TREX-QCLAS. Accordingly, with respect to instrumental sensitivity, the technique presented here is distinctly superior to previous approaches (Harris et al., 2017; Ibraim et al., 2019; Wolf et al., 2015), yielding clearly more precise and accurate  $\text{N}_2\text{O}$  source signatures. In addition, using flux chambers allowed allocating obtained  $\text{N}_2\text{O}$  source processes in space and time, which can be interpreted more closely with respect to soil characteristics (e.g., WFPS) and nutrient availability ( $\text{NH}_4^+$ ,  $\text{NO}_3^-$ ).

As a result of BRM's topography (the site is on top of a small hill; see section 2.1.1), unlike in the aforementioned studies,  $\text{N}_2\text{O}$  did not accumulate in the NBL during the period of this study. Therefore, variability in  $\text{N}_2\text{O}$  concentrations and  $\text{N}_2\text{O}$   $\delta$  values from the 2 m inlet were not significantly different from background measurements (black and green box-plots in Figure 2) and did not allow for reliable Keeling plot analysis.

In this study Keeling plot analysis used an individual background (Time 0) and two consecutive (45 and 90 min after chamber closure) chamber headspace measurements. To evaluate the potential for a further increase in temporal resolution of the sampling technique, we investigated the following scenarios: (i) the use of mean background measurement values instead of using individual background values and (ii) the use of one analysis of chamber headspace air (45 min) in combination with

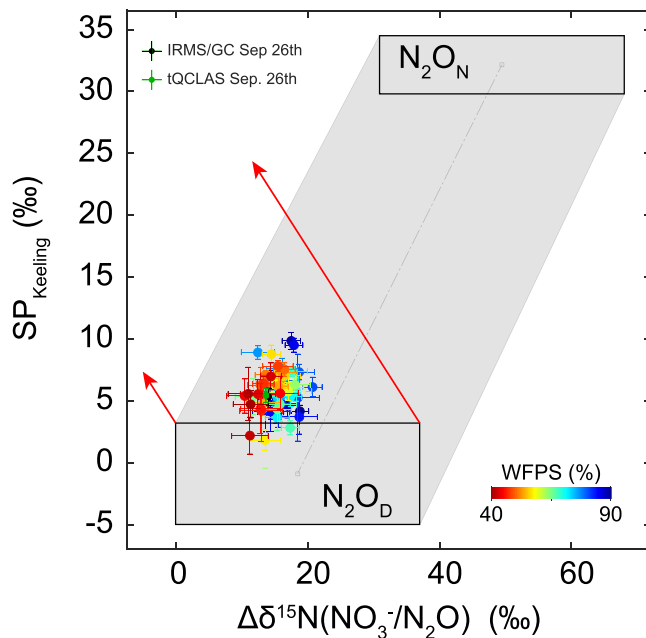


**Figure 4.** SP versus  $\Delta\delta^{15}\text{N}^{\text{bulk}}(\text{NO}_3^-/\text{N}_2\text{O})$  source signature map for the period before fertilizer addition (29 August to 5 November 2017). The  $\text{N}_2\text{O}_\text{D}$  (nitrifier-denitrification and denitrification) and  $\text{N}_2\text{O}_\text{N}$  (nitrification, abiotic  $\text{N}_2\text{O}$  production, and fungal denitrification) boxes indicate the region of  $\text{N}_2\text{O}$  source signatures from the related processes. The gray shaded area represents the region of source signatures expected for a mix of  $\text{N}_2\text{O}_\text{N}$  and  $\text{N}_2\text{O}_\text{D}$ , while red arrows indicate changes in the source signatures due to partial  $\text{N}_2\text{O}$  reduction. Indicated values correspond to obtained mean  $\pm 1$  SD values, and the color trend indicates the corresponding water filled pore space (WFPS) values.

90% WFPS and decreasing  $\text{N}_2\text{O}$  fluxes beyond 90% WFPS (Ibraim et al., 2019; Lewicka-Szczebak et al., 2017). High WFPS favors anoxic conditions and thereby bacterial denitrification, thus high  $\text{N}_2\text{O}$  fluxes (Schindlbacher et al., 2004; Toyoda et al., 2011). However, at WFPS values close to saturation (i.e., >90%), diffusion of  $\text{N}_2\text{O}$  from soil to atmosphere is suppressed. Moreover, under such conditions, the share of complete denitrification is higher due to low oxygen availability, ultimately leading to higher  $\text{N}_2$  production and lower  $\text{N}_2\text{O}$  emissions.  $\text{N}_2\text{O}$  emissions were further affected by the soil temperature ( $p$  value <0.001), which is due to the temperature-dependent rates of microbial  $\text{N}_2\text{O}$  production (Butterbach-Bahl et al., 2013; Schindlbacher et al., 2004).

SP values of  $\text{N}_2\text{O}$  emitted from grassland soils observed in previous studies ranged from 0–35‰ (Ibraim et al., 2019; Wolf et al., 2015). In contrast, in the present study the SP values were between 1.8‰ and 9.8‰, resulting in a mean value of  $5.8\text{‰} \pm 1.6$  (Figures 4 and 5). As discussed in detail in section 4.3, low SP values are a strong indication that the  $\text{N}_2\text{O}_\text{D}$  domain has predominantly contributed to the observed  $\text{N}_2\text{O}$  emissions (Decock & Six, 2013). Occasional increases in SP may be explained as an initialization of complete denitrification (Friedl et al., 2016; Lewicka-Szczebak et al., 2017) or as a temporal increase in the relative contribution of nitrification to total  $\text{N}_2\text{O}$  emission. In the first week of September, after heavy rainfalls between 30 August and 2 September, an increase of WFPS values beyond 90% was observed. In this case, an initialization of complete denitrification is most likely.

Environmental controls on  $\delta^{18}\text{O}-\text{N}_2\text{O}$  are especially important, since SP versus  $\delta^{18}\text{O}-\text{N}_2\text{O}$  mapping has been proposed as a means for calculating the share of  $\text{N}_2\text{O}$  that has been reduced to  $\text{N}_2$ , which is a prerequisite for source partitioning to the process groups  $\text{N}_2\text{O}_\text{N}$  and  $\text{N}_2\text{O}_\text{D}$ . The final step of denitrification, that is,  $\text{N}_2\text{O}$  reduction to  $\text{N}_2$ , leads to an enrichment

of both  $\delta^{18}\text{O}-\text{N}_2\text{O}$  and SP. For this reason, the shift in  $\text{N}_2\text{O}$  isotopic composition due to  $\text{N}_2\text{O}$  reduction to  $\text{N}_2$  has to be considered when partitioning total  $\text{N}_2\text{O}$  emission to the process groups  $\text{N}_2\text{O}_\text{N}$  and  $\text{N}_2\text{O}_\text{D}$ . To deduce the share of  $\text{N}_2\text{O}$  that was produced in the soil, then reduced to  $\text{N}_2$  and subsequently emitted to the atmosphere, isotopomer maps have been suggested (Koba et al., 2009; Lewicka-Szczebak et al., 2017; Verhoeven et al., 2019) that show the relation of  $\delta^{18}\text{O}$  to SP. This approach assumes a stable isotopic composition of  $\text{N}_2\text{O}$  originating from process group  $\text{N}_2\text{O}_\text{D}$  with regard to SP and  $\delta^{18}\text{O}$  and interprets deviations from this composition with respect to  $\text{N}_2\text{O}$  reduction. This might be a robust assumption as the associated N intermediates of the  $\text{N}_2\text{O}$  precursor,  $\text{NO}_3^-$ , exchange oxygen with soil water, which stabilizes the precursor isotopic composition against fractionation due to nitrification (production), denitrification (consumption), and other fractionating processes such as microbial immobilization or plant uptake. For this reason, however, systematic effects on  $\delta^{18}\text{O}-\text{N}_2\text{O}$  other than  $\text{N}_2\text{O}$  reduction need to be identified. During the campaign, WFPS ranged from 40 to 95%. Over this WFPS range,  $\delta^{18}\text{O}-\text{N}_2\text{O}$  decreased from approximately 45‰ to 30‰ (Figure 3) and showed a significant negative correlation ( $p < 0.001$ ). Since high WFPS is caused by precipitation, and  $\delta^{18}\text{O}$  of precipitation is depleted compared to  $\delta^{18}\text{O}-\text{N}_2\text{O}$  ( $\delta^{18}\text{O}-\text{H}_2\text{O}_{\text{precip}}$  varies between  $-10\text{‰}$  and  $-3\text{‰}$  according to Mook, 2001), this correlation indicates a high oxygen exchange rate between soil water and  $\text{NO}_3^-$ . This phenomenon, also known from previous laboratory scale studies, is indicated by replacing  $\delta^{18}\text{O}-\text{N}_2\text{O}$  by  $\Delta\delta^{18}\text{O}(\text{H}_2\text{O}/\text{N}_2\text{O})$  as the difference of  $\delta^{18}\text{O}$  values between the soil water ( $\delta^{18}\text{O}-\text{H}_2\text{O}$ ) and the product ( $\delta^{18}\text{O}-\text{N}_2\text{O}$ ) (Lewicka-Szczebak et al., 2014; Lewicka-Szczebak et al., 2016; Well et al., 2008; Zhu et al., 2013). The enrichment of  $\Delta\delta^{18}\text{O}(\text{H}_2\text{O}/\text{N}_2\text{O})$  during drying or dry periods (Figures 3 and S9) supports the notion that besides  $\text{N}_2\text{O}$  reduction, evaporative  $^{18}\text{O}$ -enrichment of  $\delta^{18}\text{O}-\text{H}_2\text{O}_{\text{soil water}}$  affects  $\Delta\delta^{18}\text{O}(\text{H}_2\text{O}/\text{N}_2\text{O})$  values, which is also in accordance with previous observations (Benettin et al., 2018; Kayler et al., 2018; Sprenger et al., 2017). This indicates that, in summary, the variability of  $\Delta\delta^{18}\text{O}(\text{H}_2\text{O}/\text{N}_2\text{O})$  can be explained by the effects of (i) mixing of precipitation water and soil water with subsequent

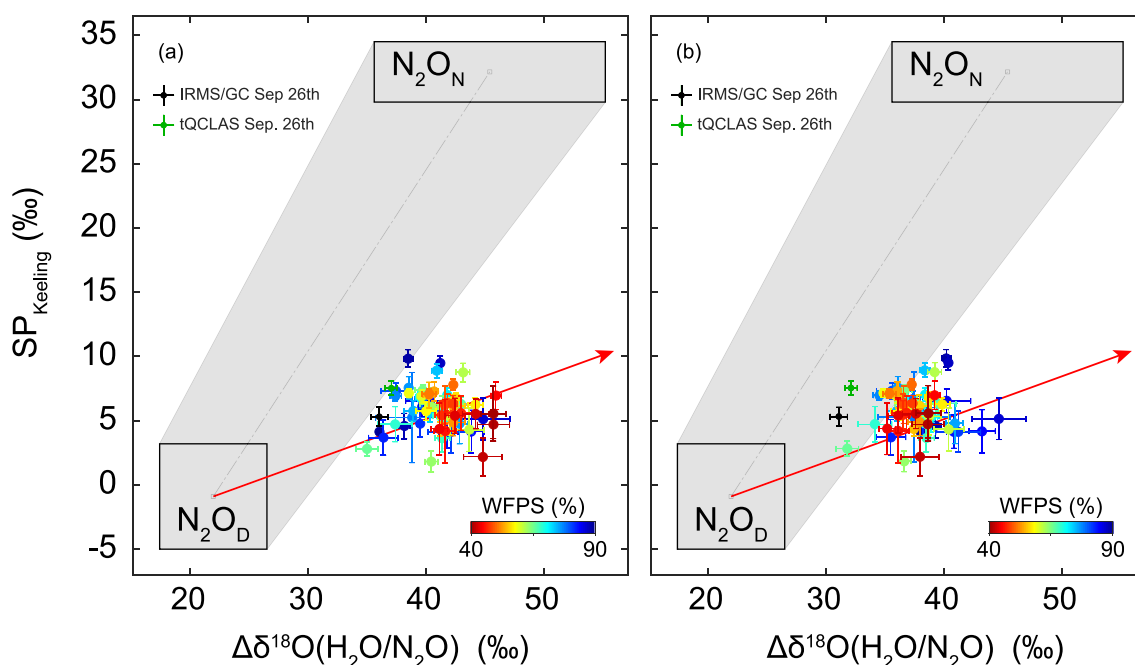


**Figure 5.** Source signature maps for the period before fertilizer addition (29 August to 5 November 2017) with the  $\Delta\delta^{18}\text{O}$  approach according to Lewicka-Szczebak et al. (2017). The  $\text{N}_2\text{O}_\text{D}$  (nitrifier-denitrification and denitrification) and  $\text{N}_2\text{O}_\text{N}$  (nitrification, abiotic  $\text{N}_2\text{O}$  production, and fungal denitrification) boxes indicate the region of  $\text{N}_2\text{O}$  source signatures from the related processes (a compilation of literature values can be found in Ibraim et al., 2019). The gray shaded area represents the region of source signatures expected for a mix of  $\text{N}_2\text{O}_\text{N}$  and  $\text{N}_2\text{O}_\text{D}$ , while red arrows indicate changes in the source signatures due to partial  $\text{N}_2\text{O}$  reduction. (a) Before correction of  $\delta^{18}\text{O}$ - $\text{N}_2\text{O}$  values for WFPS and (b) after correction for WFPS according to Equation 4. The color trend refers to observed water filled pore space (WFPS) as indicated. For 26 September, IRMS results are given in addition to the TREX-QCLAS results.

oxygen exchange between soil water and  $\text{NO}_3^-$ , (ii) evaporative  $^{18}\text{O}$ -enrichment of soil water and propagation of  $^{18}\text{O}$  enriched water to  $\text{NO}_3^-$ , and (iii)  $\text{N}_2\text{O}$  reduction on  $\Delta\delta^{18}\text{O}(\text{H}_2\text{O}/\text{N}_2\text{O})$ .

### 4.3. Source Signatures of Soil-Emitted $\text{N}_2\text{O}$ and Implicated Processes

Two end-member mapping approaches were proposed based on (i) SP versus  $\delta^{15}\text{N}^{\text{bulk}}\text{-N}_2\text{O}$  and (ii) SP versus  $\Delta\delta^{18}\text{O}(\text{H}_2\text{O}/\text{N}_2\text{O})$  as a means for identifying  $\text{N}_2\text{O}$  emitting source processes (Koba et al., 2009; Sutka et al., 2006; Sutka et al., 2008; Toyoda et al., 2005). Because SP is thought to be independent of the isotopic composition of the precursors  $\text{NH}_4^+$  and  $\text{NO}_3^-$ , it is considered to be more robust in this regard than  $\delta^{15}\text{N}^{\text{bulk}}$  and  $\delta^{18}\text{O}$ . However, due to the overlap of SP from different processes, only the process groups  $\text{N}_2\text{O}_\text{D}$  and  $\text{N}_2\text{O}_\text{N}$  can be distinguished with this parameter. In addition, source partitioning based on a single isotopic quantity (SP) does not allow a unique mathematical solution if a third process is involved. Therefore, the impact of the final process step of denitrification,  $\text{N}_2\text{O}$  reduction to  $\text{N}_2$ , which increases SP, needs to be considered while partitioning  $\text{N}_2\text{O}_\text{D}$  and  $\text{N}_2\text{O}_\text{N}$  source contributions. To this end, isotope maps as shown in Figures 4 and 5 have been proposed (Koba et al., 2009; Lewicka-Szczebak et al., 2017). The basic assumption of these approaches is that there are characteristic isotopic compositions for the process groups  $\text{N}_2\text{O}_\text{N}$  and  $\text{N}_2\text{O}_\text{D}$ , and  $\text{N}_2\text{O}$  to  $\text{N}_2$  reduction displays a constant  $\text{SP}/\delta^{15}\text{N}^{\text{bulk}}$  or  $\text{SP}/\delta^{18}\text{O}$  ratio (derivation of the black boxes from literature as explained by Ibraim et al., 2019). The  $\text{N}_2\text{O}_\text{N}$  and  $\text{N}_2\text{O}_\text{D}$  source signatures'  $\delta^{15}\text{N}^{\text{bulk}}$  values are calculated as the difference between the precursors' and  $\text{N}_2\text{O}$ 's  $\delta^{15}\text{N}$  values, that is, between  $\delta^{15}\text{N}\text{-NO}_3^-$ ,  $\delta^{15}\text{N}\text{-NH}_4^+$ , and  $\delta^{15}\text{N}^{\text{bulk}}\text{-N}_2\text{O}$ . The implementation of this procedure is indicated by replacing  $\delta^{15}\text{N}^{\text{bulk}}$  by either  $\delta^{15}\text{N}^{\text{bulk}}(\text{no}_3^-/\text{n}_2\text{o})$  or  $\delta^{15}\text{N}^{\text{bulk}}(\text{nh}_4^+/\text{n}_2\text{o})$ , depending on the anticipated dominant precursor.

#### 4.3.1. Interpretation of Obtained Source Signatures With the SP Versus $\Delta^{15}\text{N}^{\text{bulk}}$ approach

The SP versus  $\Delta^{15}\text{N}^{\text{bulk}}$  dual-isotope maps are interpreted with respect to the mixing line between the characteristic sp and  $\Delta^{15}\text{N}^{\text{bulk}}$  domains of  $\text{n}_2\text{o}_\text{n}$  and  $\text{n}_2\text{o}_\text{d}$ . deviations from this line toward higher sp

and lower  $\Delta^{15}\text{N}^{\text{bulk}}$  values (red arrow in figure 4) indicate a shift in isotopic composition due to  $\text{N}_2\text{O}$  reduction.

The slope of the line connecting the mixing line and product  $\text{N}_2\text{O}$  is defined by the ratio of the fractionation factors for SP and  $\Delta^{15}\text{N}^{\text{bulk}}$  during  $\text{N}_2\text{O}$  reduction as introduced by Koba et al. (2009). The mean  $\Delta^{15}\text{N}^{\text{bulk}}(\text{NO}_3^-/\text{N}_2\text{O})$  source signature determined in this study corresponds to  $15.2 \pm 2.1\text{‰}$  (Figure 4), which is in agreement with  $\Delta^{15}\text{N}^{\text{bulk}}(\text{NO}_3^-/\text{N}_2\text{O})$  values presented by Ibraim et al. (2019) for an intensively managed grassland site in Southern Germany. Interestingly, the values also agree with those found in a groundwater study by Koba et al. (2009), where  $\Delta^{15}\text{N}^{\text{bulk}}(\text{NO}_3^-/\text{N}_2\text{O})$  values between 0‰ and 22‰ were observed. Compared to the  $\Delta^{15}\text{N}^{\text{bulk}}(\text{NO}_3^-/\text{N}_2\text{O})$  values, the  $\Delta^{15}\text{N}^{\text{bulk}}(\text{NH}_4^+/\text{N}_2\text{O})$  values (not shown) were offset by +4.8‰. They are not discussed further due to the observed predominance of denitrification-derived  $\text{N}_2\text{O}$ .

In contrast to  $\Delta^{15}\text{N}^{\text{bulk}}$  values, the observed SP values were distinctly more confined, clustering close to the  $\text{N}_2\text{O}_\text{D}$  domain at 1.8‰ to 9.8‰, than SP signatures found in the aforementioned surveys (Ibraim et al., 2019; Wolf et al., 2015), where SP values ranged between 0‰ and 35‰. The average SP source signature of  $5.8 \pm 1.6\text{‰}$  is around 7‰ higher than that expected from pure bacterial denitrification (Sutka et al., 2006). Based on the graphical approach presented in Figure 4, we found that 30–55% of produced  $\text{N}_2\text{O}$  was reduced to  $\text{N}_2$ . The share of  $\text{N}_2\text{O}_\text{N}$ -derived  $\text{N}_2\text{O}$  amounted to 3–18%. Related values are given in Table S3 in more detail.

#### 4.3.2. Interpretation of Obtained Source Signatures With the SP Versus $\delta^{18}\text{O}(\text{H}_2\text{O}/\text{N}_2\text{O})$ approach

To further confine the share of  $\text{N}_2\text{O}$  reduction, Lewicka-Szczebak et al. (2017) introduced the approach based on SP versus  $\Delta\delta^{18}\text{O}(\text{H}_2\text{O}/\text{N}_2\text{O})$ . In this approach,  $\Delta\delta^{18}\text{O}(\text{H}_2\text{O}/\text{N}_2\text{O})$  is calculated as the difference of  $\delta^{18}\text{O}$  values between the product ( $\text{N}_2\text{O}$ ) and soil water ( $\text{H}_2\text{O}$ ). Since no measurements for the  $\delta^{18}\text{O}-\text{H}_2\text{O}$  values of soil water were available, we used an average  $\delta^{18}\text{O}-\text{H}_2\text{O}$  value of  $-7\text{‰}$  as reported by Feng et al. (2009). An advantage of the Lewicka-Szczebak et al. (2017) approach is that the range of  $\delta^{18}\text{O}(\text{H}_2\text{O}/\text{N}_2\text{O})$  values is distinctly smaller, reducing the size of the  $\text{N}_2\text{O}_\text{D}$  box in Figure 5. There are two scenarios that could lead to the final observed  $\text{N}_2\text{O}$  isotopic composition. The first scenario assumes partial reduction of  $\text{N}_2\text{O}_\text{D}$  followed by mixing with  $\text{N}_2\text{O}_\text{N}$ , while the second pathway assumes mixing of  $\text{N}_2\text{O}_\text{D}$  and  $\text{N}_2\text{O}_\text{N}$ , followed by  $\text{N}_2\text{O}$  reduction. Although it is not possible to identify which scenario is more appropriate, this approach constrained the share of  $\text{N}_2\text{O}$  originating from  $\text{N}_2\text{O}_\text{N}$  to a range of 2–20%. The share of the produced  $\text{N}_2\text{O}$  further reduced to  $\text{N}_2$  was 30–70% according to the Rayleigh equation  $\text{SP} = \text{SP}_0 + \epsilon_{\text{SP}} * \ln(r\text{N}_2\text{O})$  (Lewicka-Szczebak et al., 2017; Mariotti et al., 1981) with  $r\text{N}_2\text{O}$  being the residual fraction of  $\text{N}_2\text{O}$  and using an average enrichment factor,  $\epsilon_{\text{SP}} = -5.9\text{‰}$ , in accordance with Ostrom et al. (2007). Therefore, we conclude that, at BRM, the observed SP shift was caused by  $\text{N}_2\text{O}$  reduction to  $\text{N}_2$  rather than by a contribution of  $\text{N}_2\text{O}_\text{N}$ .

Based on the SP versus  $\delta^{18}\text{O}(\text{H}_2\text{O}/\text{N}_2\text{O})$  method, the share of  $\text{N}_2\text{O}_\text{D}$  and  $\text{N}_2\text{O}_\text{N}$  can be derived as explained above. However, this method was developed for studies under controlled conditions, implying complete O-exchange between soil water and N-precursors ( $\text{NO}_3^-$ ) of denitrification. Hence, the two process domains  $\text{N}_2\text{O}_\text{D}$  and  $\text{N}_2\text{O}_\text{N}$  together with  $\text{N}_2\text{O}$  reduction to  $\text{N}_2$  are assumed to be the only parameters influencing the final observed SP and  $\delta^{18}\text{O}(\text{H}_2\text{O}/\text{N}_2\text{O})$  values. In contrast, as outlined in section 4.2, evaporative  $^{18}\text{O}$  enrichment (Benettin et al., 2018; Kayler et al., 2018; Sprenger et al., 2017) and the extent of O exchange between soil water and precipitation (Lewicka-Szczebak et al., 2014; Lewicka-Szczebak et al., 2016; Well et al., 2008; Zhu et al., 2013) may have systematically influenced the observed  $\delta^{18}\text{O}(\text{H}_2\text{O}/\text{N}_2\text{O})$  values in this study, because we observed a wide range of WFPS values during the measurement campaign. This is based on the notion that nitrification played a minor role during the measurement campaign and that increases in WFPS should be accompanied with enrichment in  $\delta^{18}\text{O}(\text{H}_2\text{O}/\text{N}_2\text{O})$  due to an increasing share of  $\text{N}_2\text{O}$  reduction to  $\text{N}_2$ , which however was in contrast to observations. Consequently, the share of  $\text{N}_2\text{O}_\text{N}$  and the rate of  $\text{N}_2\text{O}$  reduction to  $\text{N}_2$  presented above may be biased due to low  $\delta^{18}\text{O}(\text{H}_2\text{O}/\text{N}_2\text{O})$  end-member values (actual  $\delta^{18}\text{O}(\text{H}_2\text{O}/\text{N}_2\text{O})$  end-member values are assumed to be higher due to evaporative  $^{18}\text{O}$  enrichment in soil water and incomplete  $^{18}\text{O}$  exchange with  $\text{NO}_3^-$ ). To deduce the influence of evaporative  $^{18}\text{O}$  enrichment and O exchange, we applied a statistical correction following Equation 4:

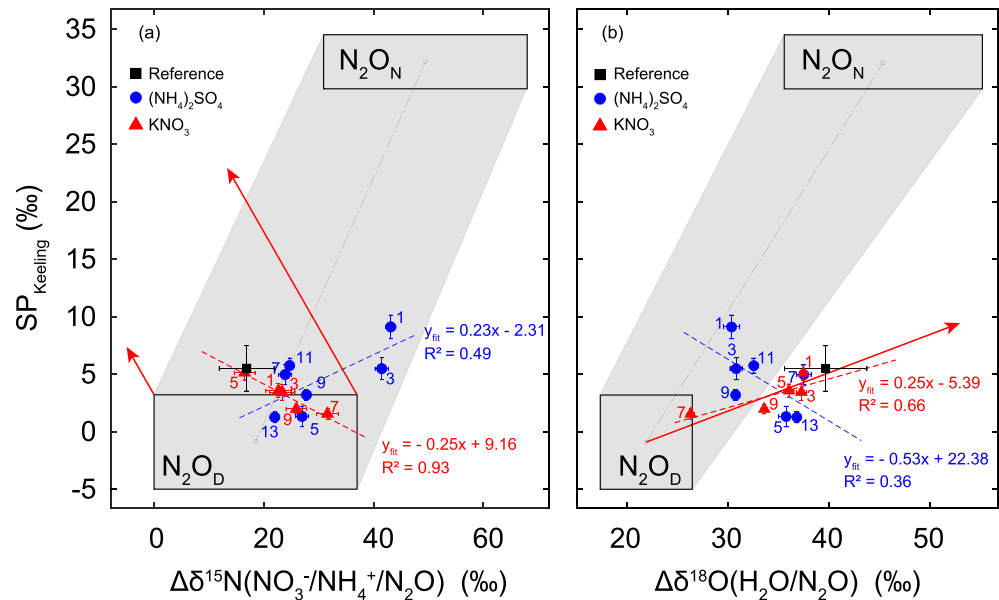


**Figure 6.** Source signature maps for the period after fertilizer addition (6 November to 1 December 2017). The  $N_2O_D$  (nitrifier-denitrification and denitrification) and  $N_2O_N$  (nitrification, abiotic  $N_2O$  production, and fungal denitrification) boxes indicate the region of  $N_2O$  source signatures from the related processes (a compilation of literature values can be found in Ibraim et al., 2019). The gray shaded area represents the region of source signatures expected for a mix of  $N_2O_N$  and  $N_2O_D$ , while red arrows indicate direction of changes in the source signatures due to partial  $N_2O$  reduction. Blue dots represent measurements during  $(NH_4)_2SO_4^-$  addition experiments, while red triangles depict measurements during  $KNO_3$  addition experiments. Given numbers refer to number of days after fertilizer addition. Blue and red dashed lines represent linear fits of obtained source signatures. (a) SP versus  $\Delta\delta^{15}N^{bulk}(NO_3^-/NH_4^+/N_2O)$  map, where fertilizer  $\delta^{15}N^{bulk}-NO_3^-$  and  $\delta^{15}N^{bulk}-NH_4^+$  values were included to determine net isotope effects and (b) SP versus  $\Delta\delta^{18}O(H_2O/N_2O)$  map as introduced earlier.

$$\Delta\delta^{18}O(H_2O/N_2O)_{corr} = \Delta\delta^{18}O(H_2O/N_2O_{Keeling}) - \Delta\delta^{18}O - (H_2O/N_2O)_{Fit} + \Delta\delta^{18}O - (H_2O/N_2O)_{90\%WFPS} \quad (4)$$

In Equation 4,  $\Delta\delta^{18}O(H_2O/N_2O_{Keeling})$  corresponds to the Keeling plot-derived  $\Delta\delta^{18}O(H_2O/N_2O)$  values. The term  $\Delta\delta^{18}O - (H_2O/N_2O)_{Fit}$  depicts the fitted values at given WFPS as following the two-term exponential fit introduced in section 3.2.1. The term  $\Delta\delta^{18}O - (H_2O/N_2O)_{90\%WFPS}$  equals 37.1‰ and represents the fitted  $\Delta\delta^{18}O(H_2O/N_2O)$  value at 90% WFPS, thus depicting the characteristic bacterial denitrification-derived  $\Delta\delta^{18}O(H_2O/N_2O)$  value at BRM.

Thus, the corrected  $\Delta\delta^{18}O(H_2O/N_2O)$  values may be less vulnerable toward systematic influences of evaporative  $^{18}O$  enrichment or incomplete O exchange and isolate the effect of  $N_2O$  reduction to  $N_2$ . The average  $\Delta\delta^{18}O(H_2O/N_2O)$  values were  $34.0 \pm 2.4\text{‰}$  and  $30.7 \pm 2.2\text{‰}$  before and after the correction. Using the corrected  $\delta^{18}O-N_2O$  values, the share of  $N_2O_N$ -derived  $N_2O$  corresponded to 6–14% (Table S3). This is well within the range of values (3–18%) obtained without correction. The share of  $N_2O$  reduction to  $N_2$  based on the corrected values amounts to 30–55%, which is 9% to 10% lower than prior to the correction. Since the standard deviation of the Keeling plot-derived  $\delta^{18}O$  values is around 2‰, half of the average correction, the influence of evaporative enrichment or efficiency of exchange with water, on the share of  $N_2O$  reduced to  $N_2$ , is rather moderate.

Even though the presented approach represents current best practice, assuming constant fractionation factors might be an oversimplification, as it has been previously shown that fractionation factors change over time (Jinuntuya-Nortman et al., 2008). Furthermore, additional  $N_2O$  source processes, for example, fungal denitrification and chemodenitrification (implying increased SP values), could not be specifically addressed here (Denk et al., 2017; Wei et al., 2019). Nevertheless source signatures at BRM are consistent with previous findings from open system studies (Ibraim et al., 2019; Mohn et al., 2012; Mohn et al., 2013; Verhoeven



et al., 2019; Wolf et al., 2015; Yamamoto et al., 2014), revealing that  $\text{N}_2\text{O}$  reduction to  $\text{N}_2$  was the main factor determining observed  $\text{N}_2\text{O}$  source signatures. Depending on WFPS, 30–70% of produced  $\text{N}_2\text{O}$  was reduced to  $\text{N}_2$  before emission of remaining  $\text{N}_2\text{O}$  to the atmosphere.

#### 4.3.3. Interpretation of Obtained Source Signatures After $(\text{NH}_4)_2\text{SO}_4$ and $\text{KNO}_3$ Addition

Fertilization with  $70 \text{ kg N ha}^{-1}$   $(\text{NH}_4)_2\text{SO}_4$  should promote  $\text{N}_2\text{O}$  production via nitrification due to the enhanced  $\text{NH}_4^+$  availability, ultimately leading to a shift of the  $\text{N}_2\text{O}$  source signatures toward the  $\text{N}_2\text{O}_\text{N}$  domain (Decock & Six, 2013; Robertson & Groffman, 2015). Indeed, on the first day after the fertilizer addition, an increase in SP (pointing toward the  $\text{N}_2\text{O}_\text{N}$  domain) together with a strong increase of the  $\Delta\delta^{15}\text{N}^{\text{bulk}}$  values was observed, indicating that the applied  $(\text{NH}_4)_2\text{SO}_4$  effectively enhanced  $\text{N}_2\text{O}$  production by the nitrification pathway. The fertilization effect was still visible on Day 3 after  $(\text{NH}_4)_2\text{SO}_4$  addition but decreased over time, and the difference between treatment and reference chambers disappeared at Days 5, 7, 9, 11, and 13 (Figure 6). Thus, we conclude that the addition of  $(\text{NH}_4)_2\text{SO}_4$  caused a shift of the  $\text{N}_2\text{O}$  emitting soil processes toward the  $\text{N}_2\text{O}_\text{N}$  domain, while it leaves open whether nitrification or fungal denitrification was primarily causing the shift. Nevertheless, the highest  $\text{N}_2\text{O}$  emission was observed on Day 1 after fertilization, when  $\text{NH}_4^+$  concentrations were also at their climax. On Days 3 and 5 after fertilization, both  $\text{N}_2\text{O}$  emission and  $\text{NH}_4^+$  concentrations in the soil decreased while  $\text{NO}_3^-$  concentrations reached their maximum, which suggests that the observed emissions may have been rather due to substrate induced nitrification than fungal denitrification. This notion is supported by the decrease of  $\text{N}_2\text{O}$  emission at increasing  $\text{NO}_3^-$  availability as most fungi are not capable to reduce  $\text{N}_2\text{O}$  to  $\text{N}_2$  (Shoun et al., 1992). After the emission pulse, that is, from Day 5 after  $(\text{NH}_4)_2\text{SO}_4$  addition, the  $\text{N}_2\text{O}$  source signatures suggest that denitrification was the dominating  $\text{N}_2\text{O}$  producing process with regard to background emission. As indicated in Figure 6, they were falling on lines with the slopes 0.23 and  $-0.53$  in the SP versus  $\Delta\delta^{15}\text{N}^{\text{bulk}}$  and SP versus  $\Delta\delta^{18}\text{O}(\text{H}_2\text{O}/\text{N}_2\text{O})$  end-member mixing maps, respectively.

Addition of  $\text{KNO}_3$  led to source signatures falling on a line that connects the average source signatures from the reference chambers with the  $\text{N}_2\text{O}_\text{D}$  domain, indicating that the high share of denitrification-derived  $\text{N}_2\text{O}$  was increased even further. The related  $R^2$  values of 0.93 and 0.66 with the two mapping approaches indicate a high degree of consistency in the represented processes. The slope of 0.25 in the SP versus  $\Delta\delta^{18}\text{O}(\text{H}_2\text{O}/\text{N}_2\text{O})$  map is very close to the slope derived with incubation studies by Lewicka-Szczebak et al. (2017). Addition of  $\text{KNO}_3$  (i.e., inducing conditions that favor pure bacterial denitrification) led to slightly lower SP values compared to the SP values obtained prior to the  $\text{KNO}_3$  addition. This seems plausible because the reference SP value was already very close to that expected from pure bacterial denitrification. Since the  $\text{KNO}_3$  was applied with 22 mm water, in the first days after the  $\text{KNO}_3$  application, the oxygen availability was limited due to high soil water content. Accordingly, obtained source signatures indicate a higher rate of  $\text{N}_2\text{O}$  reduction to  $\text{N}_2$  in the first days after  $\text{KNO}_3$  addition. At Days 7 and 9, the oxygen availability slightly increased as a result of decreasing WFPS, ultimately leading to SP values that are very close to those of bacterial denitrification in the absence of  $\text{N}_2\text{O}$  reduction.

#### 4.4. Biogeochemical and Isotopic Modeling

Comparing the measurements to the modeled results, the coefficients of determination ( $R^2$ ) of WFPS and soil temperature were high (0.86 and 0.92, respectively), and the average deviations of the observed WFPS and soil temperature were low (2.2% and 1.5 K, respectively), indicating that the LandscapeDNDC model produces a realistic representation of the soil environmental conditions. As in model-data comparisons from other studies,  $R^2$  values of 0.08–0.85 and 0.85–0.93 for WFPS and soil temperature as well as average deviations of 0.1–2.8% and 0.2–1.7 K were reported (Gaillard et al., 2018; Molina-Herrera et al., 2016; Wolf et al., 2012). Therefore, the quality of the presented simulated soil environmental conditions can be classified as high. High  $R^2$  values for measured versus simulated soil  $\text{NH}_4^+$  (0.33) and  $\text{NO}_3^-$  (0.41) concentrations are also well within the reported ranges of 0.01 to 0.98 ( $\text{NH}_4^+$ ) and 0.03 to 0.47 ( $\text{NO}_3^-$ ) for grasslands and arable sites (Molina-Herrera et al., 2016). The  $R^2$  of daily modeled versus measured  $\text{N}_2\text{O}$  emissions during the growing season was 0.26 in this study, which is well within the range of reported values (0.01–0.68) obtained in LandscapeDNDC simulations and in a model intercomparison study (Gaillard et al., 2018; Molina-Herrera et al., 2016; Wolf et al., 2012). Low  $R^2$  values for  $\text{N}_2\text{O}$  emissions are generally (including in this study) due to the bias in the timing of emission peaks and the delayed decay of peak emissions. Particularly, high

bulk densities were measured in the subsoil at BRM, which are associated with lower soil porosity and more mesopores and micropores (Balaine et al., 2016). Mesopores and micropores retain more water against a given suction head, so that anaerobic conditions occur more frequently in deeper soil layers. Anaerobic conditions stimulate denitrification, which produces  $\text{N}_2\text{O}$  as an obligate intermediate (see Butterbach-Bahl et al., 2013, and references therein). As denitrification was the predominant source of  $\text{N}_2\text{O}$  in our simulations, and anaerobic conditions occurred frequently in the subsoil of the BRM site, the slow decrease of emissions and also the overestimation of  $\text{N}_2\text{O}$  emission were likely the result of the high bulk density in the subsoil observed at BRM.

Following LandscapeDNDC application to the site, we used the simulation results on N turnover and  $\text{N}_2\text{O}$  production/emission to drive the SIMONE model. With regard to the  $\delta^{15}\text{N}^{\text{bulk}}$  measurements, LandscapeDNDC-SIMONE simulations showed a higher  $^{15}\text{N}$  enrichment of  $\text{N}_2\text{O}$  as compared to the measurements. Since  $\delta^{15}\text{N}^{\text{bulk}}$  directly depends on the isotopic composition of the precursors and  $\text{NO}_3^-$  was the predominant substrate for  $\text{N}_2\text{O}$  formation in the model, overestimation of  $^{15}\text{N}$ -enrichment in  $\text{NO}_3^-$  could explain the difference. However, the comparison of measured and modeled  $\delta^{15}\text{N}\text{-NO}_3^-$  showed only small deviations before the fertilization experiments, so that the isotope effect for denitrification used within SIMONE may be too weak. The enrichment of the  $\text{NH}_4^+$  pool was distinctly overestimated by the model (Figure S11), which may have added to the too high enrichment in  $\delta^{15}\text{N}^{\text{bulk}}$ , though  $\text{NH}_4^+$  was only a minor source of  $\text{N}_2\text{O}$ . The strong enrichment of the  $\text{NH}_4^+$  pool suggests that mineralization may be underestimated compared to the nitrification rate.

The less-pronounced decrease of  $\delta^{15}\text{N}\text{-N}_2\text{O}$  after the first fertilizer application indicates that the amount of N transformed by microorganisms was underestimated, which is in line with the missing reduction in soil  $\text{NH}_4^+$ , and indicates that the temperature limitation of microbial N turnover and plant growth in LandscapeDNDC needs to be revisited.

#### 4.4.1. Source Partitioning by Isotope Analysis and LandscapeDNDC-SIMONE

Although other recent studies including in situ measurements of SP from grassland and agricultural systems based on QCLAS (Harris et al., 2015; Ibraim et al., 2019; Wolf et al., 2015) or flask sampling with subsequent IRMS analysis (Toyoda et al., 2011) showed pronounced variability of SP over time, we observed limited variability of SP. Since the variability in SP reported in the literature could be explained by changing contributions of  $\text{N}_2\text{O}$  producing processes, or changing degrees of  $\text{N}_2\text{O}$  reduction (Ibraim et al., 2019; Lewicka-Szczebak et al., 2017; Toyoda et al., 2011; Verhoeven et al., 2019), the lack of variability in our measurements and simulations indicates that there was a dominant combination of processes that prevailed throughout the campaign. The consistently low SP suggests that the main source of  $\text{N}_2\text{O}$  was denitrification or nitrifier denitrification, as a SP of approximately  $-0.9\text{‰}$  has been observed for this process group. Though nitrifier denitrification cannot be ruled out entirely, the high soil bulk densities and the associated higher probability of anaerobic conditions in the soil indicate that bacterial denitrification was more likely the dominant  $\text{N}_2\text{O}$ -producing process. The location of the measurements in  $\text{SP-}\Delta\delta^{18}\text{O}$  space (Figure 5a) relative to a simple mixing of  $\text{N}_2\text{O}$  produced by the process groups  $\text{N}_2\text{O}_\text{D}/\text{N}_2\text{O}_\text{N}$  can be used to estimate the contribution of  $\text{N}_2\text{O}$  reduction and nitrification to the observed isotopic composition (Lewicka-Szczebak et al., 2017). According to this approach, the process group  $\text{N}_2\text{O}_\text{N}$  contributed on average  $3 \pm 4\%$  assuming Scenario 1 (first reduction, then mixing of the  $\text{N}_2\text{O}$  derived from the domains  $\text{N}_2\text{O}_\text{N}$  and  $\text{N}_2\text{O}_\text{D}$ ) and  $18 \pm 3\%$  assuming Scenario 2 (first mixing, then reduction), accordingly leading to a  $\text{N}_2\text{O}_\text{D}$  contribution of approximately 82–97%.

This is in general agreement with the calculated percentages of (i) 72%  $\text{N}_2\text{O}$  reduction for a scenario in which exclusively  $\text{N}_2\text{O}$  reduction with an isotope effect of  $-5.9\text{‰}$  shifts SP from the  $-0.9\text{‰}$  of process group  $\text{N}_2\text{O}_\text{D}$  to the observed average SP of  $5.8\text{‰}$  and (ii) a maximum contribution of 20% for nitrification, assuming no  $\text{N}_2\text{O}$  reduction and endmembers of  $-0.9\text{‰}$  and  $32.8\text{‰}$  for the process groups  $\text{N}_2\text{O}_\text{D}$  and  $\text{N}_2\text{O}_\text{N}$ , respectively. In the LandscapeDNDC simulations, 7% of  $\text{N}_2\text{O}$  was produced on average during nitrification (range of 1.8% to 17%), and an average of 30% (range 18–47%) of the produced  $\text{N}_2\text{O}$  was reduced to  $\text{N}_2$  (Figure S12). While the low modeled contribution of nitrification together with the lower modeled share of  $\text{N}_2\text{O}$  reduction explains the underestimation of SP by  $4.2\text{‰}$ , the total  $\text{N}_2\text{O}$  emission has to be taken into account as well. The modeled  $\text{N}_2\text{O}$  emissions were on average  $190 \mu\text{g N}_2\text{O m}^{-2} \text{ hr}^{-1}$  larger than the measured emissions. This might be due to an overestimation of  $\text{N}_2\text{O}$  production by denitrification or an underestimation of

N<sub>2</sub>O to N<sub>2</sub> reduction by the model. A reduction of N<sub>2</sub>O production during denitrification by 50% results in a contribution of nitrification of 13% and still produces an underestimation of the average SP by approximately 3‰. Consequently, such a large discrepancy cannot be explained by the too high source strength of denitrification alone. Since the location of the measurements in SP-Δδ<sup>18</sup>O space suggests a substantial contribution of N<sub>2</sub>O reduction, LandscapeDNDC most likely underestimates the amount of N<sub>2</sub>O reduced to N<sub>2</sub>.

## 5. Conclusions

To the best of our knowledge this study reports the first in situ time series of N<sub>2</sub>O source signatures (SP, δ<sup>15</sup>N<sup>bulk</sup>, and δ<sup>18</sup>O) emitted from an intensively managed grassland at daily resolution. This was possible by combining automated chamber measurements, laser spectroscopy, and preconcentration with concurrent measurements of the isotopic composition of N<sub>2</sub>O and its precursors.

We observed that N<sub>2</sub>O fluxes were highly correlated with soil water filled pore space (WFPS) and with ambient temperatures. Based on the combined analysis of N<sub>2</sub>O isotopic composition and <sup>15</sup>N abundance of the N<sub>2</sub>O precursors NO<sub>3</sub><sup>−</sup> and NH<sub>4</sub><sup>+</sup>, we found that bacterial denitrification was the main N<sub>2</sub>O-emitting process over the 3-month measurement period. Even when (NH<sub>4</sub>)<sub>2</sub>SO<sub>4</sub><sup>−</sup> was added, the share of nitrification-derived N<sub>2</sub>O remained small (<20%) and occurred only in the first 3 days after addition. This dominance of denitrification was likely due to the subsequent use of nitrification-derived NO<sub>3</sub><sup>−</sup> as substrate for N<sub>2</sub>O production via denitrification.

The comparison of modeled and measured N<sub>2</sub>O isotopic composition demonstrated the high quality of the process parameterization in LandscapeDNDC since the simulations generally reflected the temporal dynamics and features of the measurements. Nevertheless, the juxtaposition of observed and modeled N<sub>2</sub>O and NH<sub>4</sub><sup>+</sup> signatures in combination with the observed and modeled N<sub>2</sub>O fluxes suggests that LandscapeDNDC (i) overestimates nitrification and N<sub>2</sub>O production during denitrification in heavily textured soils, (ii) underestimates N<sub>2</sub>O reduction to N<sub>2</sub>, and (iii) underestimates rates of tightly linked mineralization and microbial immobilization. Hence, future research aiming at improving process-based biogeochemical models will benefit from colocating the presented in situ determination of (natural abundance) N<sub>2</sub>O isotopic composition with <sup>15</sup>N-tracing approaches that are capable of providing information on gross rates of N cycling. In addition, the model results at the end of the growing season revealed weaknesses in plant and microbial activity parameterization at low temperatures calling for extending observation periods beyond the growing season.

## Data Availability Statement

Data sets of the present study can be found in the supporting information and online (<https://doi.org/10.17605/OSF.IO/KUN23>).

## Acknowledgments

The presented study was financially supported by the Swiss National Science Foundation within Grants 200021L\_150237 and 200020L\_172585/1 and the German Research Foundation within Grants BU 1173/15-1 and ZE 1006/2-1. Marc Schwärzel, Simon Wyss, and Simon Scheidegger are acknowledged for their technical support during the Beromünster field campaign. We would like to thank Dr. Roland Werner for δ<sup>15</sup>N analysis of the applied fertilizers.

## References

- Bai, E., & Houlton, B. Z. (2009). Coupled isotopic and process-based modeling of gaseous nitrogen losses from tropical rain forests. *Global Biogeochemical Cycles*, 23, GB2011. <https://doi.org/10.1029/2008GB003361>
- Balaine, N., Clough, T. J., Beare, M. H., Thomas, S. M., & Meenken, E. D. (2016). Soil gas diffusivity controls N<sub>2</sub>O and N<sub>2</sub> emissions and their ratio. *Soil Science Society of America Journal*, 80(3), 529–540. <https://doi.org/10.2136/sssaj2015.09.0350>
- Benettin, P., Volkmann, T. H. M., von Freyberg, J., Frentress, J., Penna, D., Dawson, T. E., & Kirchner, J. W. (2018). Effects of climatic seasonality on the isotopic composition of evaporating soil waters. *Hydrology and Earth System Sciences*, 22(5), 2881–2890. <https://doi.org/10.5194/hess-22-2881-2018>
- Butterbach-Bahl, K., Bagges, E. M., Dannenmann, M., Kiese, R., & Zechmeister-Boltenstern, S. (2013). Nitrous oxide emissions from soils: How well do we understand the processes and their controls? *Philosophical Transactions of the Royal Society, B: Biological Sciences*, 368(1621), 20130122. <https://doi.org/10.1098/rstb.2013.0122>
- Butterbach-Bahl, K., Gasche, R., Breuer, L., & Papen, H. (1997). Fluxes of NO and N<sub>2</sub>O from temperate forest soils: Impact of forest type, N deposition and of liming on the NO and N<sub>2</sub>O emissions. *Nutrient Cycling in Agroecosystems*, 48(1/2), 79–90. <https://doi.org/10.1023/a:1009785521107>
- Davidson, E. A., & Kanter, D. (2014). Inventories and scenarios of nitrous oxide emissions. *Environmental Research Letters*, 9(10), 105,012. <https://doi.org/10.1088/1748-9326/9/10/105012>
- Decock, C., & Six, J. (2013). How reliable is the intramolecular distribution of N<sup>15</sup> in N<sub>2</sub>O to source partition N<sub>2</sub>O emitted from soil? *Soil Biology and Biochemistry*, 65, 114–127. <https://doi.org/10.1016/j.soilbio.2013.05.012>
- Del Grosso, S. J., Parton, W. J., Mosier, A. R., Ojima, D. S., Potter, C. S., Borken, W., et al. (2000). General CH<sub>4</sub> oxidation model and comparisons of CH<sub>4</sub> oxidation in natural and managed systems. *Global Biogeochemical Cycles*, 14(4), 999–1019. <https://doi.org/10.1029/1999GB001226>

- Denk, T. R. A., Kraus, D., Kiese, R., Butterbach-Bahl, K., & Wolf, B. (2019). Constraining N cycling in the ecosystem model LandscapeDNDC with the stable isotope model SIMONE. *Ecology*, 100(5), e02675. <https://doi.org/10.1002/ecy.2675>
- Denk, T. R. A., Mohn, J., Decock, C., Lewicka-Szczepak, D., Harris, E., Butterbach-Bahl, K., et al. (2017). The nitrogen cycle: A review of isotope effects and isotope modeling approaches. *Soil Biology & Biochemistry*, 105, 121–137. <https://doi.org/10.1016/j.soilbio.2016.11.015>
- Feng, X., Faiia, A. M., & Posmentier, E. S. (2009). Seasonality of isotopes in precipitation: A global perspective. *Journal of Geophysical Research*, 114, D08116. <https://doi.org/10.1029/2008JD011279>
- Friedl, J., Scheer, C., Rowlings, D. W., McIntosh, H. V., Strazabosco, A., Warner, D. I., & Grace, P. R. (2016). Denitrification losses from an intensively managed sub-tropical pasture—Impact of soil moisture on the partitioning of N<sub>2</sub> and N<sub>2</sub>O emissions. *Soil Biology & Biochemistry*, 92, 58–66. <https://doi.org/10.1016/j.soilbio.2015.09.016>
- Gabrielle, B., Laville, P., Henault, C., Nicoulaud, B., & Germon, J. C. (2006). Simulation of nitrous oxide emissions from wheat-cropped soils using CERES. *Nutrient Cycling in Agroecosystems*, 74(2), 133–146. <https://doi.org/10.1007/s10705-005-5771-5>
- Gaillard, R. K., Jones, C. D., Ingraham, P., Collier, S., Izaurre, R. C., Jokela, W., et al. (2018). Underestimation of N<sub>2</sub>O emissions in a comparison of the DayCent, DNDC, and EPIC models. *Ecological Applications*, 28(3), 694–708. <https://doi.org/10.1002/eap.1674>
- Garratt, J. R. (1994). Review: The atmospheric boundary layer. *Earth-Science Reviews*, 37(1-2), 89–134. [https://doi.org/10.1016/0012-8252\(94\)90026-4](https://doi.org/10.1016/0012-8252(94)90026-4)
- Grote, R., Lehmann, E., Brümmer, C., Brüggemann, N., Szarzynski, J., & Kunstmann, H. (2009). Modelling and observation of biosphere-atmosphere interactions in natural savannah in Burkina Faso, West Africa. *Physics and Chemistry of the Earth, Parts A/B/C*, 34(4-5), 251–260. <https://doi.org/10.1016/j.pce.2008.05.003>
- Haas, E., Klatt, S., Frohlich, A., Kraft, P., Werner, C., Kiese, R., et al. (2013). LandscapeDNDC: A process model for simulation of biosphere-atmosphere-hydrosphere exchange processes at site and regional scale. *Landscape Ecology*, 28(4), 615–636. <https://doi.org/10.1007/s10980-012-9772-x>
- Harris, E., Henne, S., Hüglin, C., Zellweger, C., Tuzson, B., Ibraim, E., et al. (2017). Tracking nitrous oxide emission processes at a suburban site with semicontinuous, in situ measurements of isotopic composition. *Journal of Geophysical Research: Atmospheres*, 122, 1850–1870. <https://doi.org/10.1002/2016JD025906>
- Harris, E., Joss, A., Emmenegger, L., Kipf, M., Wolf, B., Mohn, J., & Wunderlin, P. (2015). Isotopic evidence for nitrous oxide production pathways in a partial nitrification-anammox reactor. *Water Research*, 83, 258–270. <https://doi.org/10.1016/j.watres.2015.06.040>
- Hörtnagl, L., Barthel, M., Buchmann, N., Eugster, W., Butterbach-Bahl, K., Díaz-Pinés, E., et al. (2018). Greenhouse gas fluxes over managed grasslands in Central Europe. *Global Change Biology*, 24(5), 1843–1872. <https://doi.org/10.1111/gcb.14079>
- Houlton, B. Z., Marklein, A. R., & Bai, E. (2015). Representation of nitrogen in climate change forecasts. *Nature Climate Change*, 5(5), 398–401. <https://doi.org/10.1038/nclimate2538>
- Ibraim, E., Harris, E., Eyer, S., Tuzson, B., Emmenegger, L., Six, J., & Mohn, J. (2018). Development of a field-deployable method for simultaneous, real-time measurements of the four most abundant N<sub>2</sub>O isotopocules. *Isotopes in Environmental and Health Studies*, 54(1), 1–15. <https://doi.org/10.1080/10256016.2017.1345902>
- Ibraim, E., Wolf, B., Harris, E., Gasche, R., Wei, J., Yu, L., et al. (2019). Attribution of N<sub>2</sub>O sources in a grassland soil with laser spectroscopy based isotopocule analysis. *Biogeosciences*, 16(16), 3247–3266. <https://doi.org/10.5194/bg-16-3247-2019>
- IPCC (2013). In T. F. Stocker, D. Qin, G.-K. Plattner, M. Tignor, S. K. Allen, J. Boschung, et al. (Eds.), *Climate Change 2013: The physical science basis. Contribution of Working Group I to the Fifth Assessment Report of the Intergovernmental Panel on Climate Change*. Cambridge, United Kingdom and New York, NY, USA: Cambridge University press.
- Jinuntuya-Nortman, M., Sutka, R. L., Ostrom, P. H., Gandhi, H., & Ostrom, N. E. (2008). Isotopologue fractionation during microbial reduction of N<sub>2</sub>O within soil mesocosms as a function of water-filled pore space. *Soil Biology & Biochemistry*, 40(9), 2273–2280. <https://doi.org/10.1016/j.soilbio.2008.05.016>
- Kayler, Z. E., Brédoire, F., McMillan, H., Barsukov, P. A., Rusalimova, O., Nikitich, P., et al. (2018). Soil evaporation and organic matter turnover in the Sub-Taiga and Forest-Steppe of southwest Siberia. *Scientific Reports*, 8(1), 10904. <https://doi.org/10.1038/s41598-018-28977-8>
- Keeling, C. D. (1958). The concentration and isotopic abundances of atmospheric carbon dioxide in rural areas. *Geochimica et Cosmochimica Acta*, 13(4), 322–334. [https://doi.org/10.1016/0016-7037\(58\)90033-4](https://doi.org/10.1016/0016-7037(58)90033-4)
- Keeling, C. D. (1961). The concentration and isotopic abundances of carbon dioxide in rural and marine air. *Geochimica et Cosmochimica Acta*, 24(3-4), 277–298. [https://doi.org/10.1016/0016-7037\(61\)90023-0](https://doi.org/10.1016/0016-7037(61)90023-0)
- Kiese, R., Heinzler, C., Werner, C., Wochele, S., Grote, R., & Butterbach-Bahl, K. (2011). Quantification of nitrate leaching from German forest ecosystems by use of a process oriented biogeochemical model. *Environmental Pollution*, 159(11), 3204–3214. <https://doi.org/10.1016/j.envpol.2011.05.004>
- Kim, Y., Seo, Y., Kraus, D., Klatt, S., Haas, E., Tenhunen, J., & Kiese, R. (2015). Estimation and mitigation of N<sub>2</sub>O emission and nitrate leaching from intensive crop cultivation in the Hae-an catchment, South Korea. *Science of the Total Environment*, 529, 40–53. <https://doi.org/10.1016/j.scitotenv.2015.04.098>
- Koba, K., Osaka, K., Tobari, Y., Toyoda, S., Ohte, N., Katsuyama, M., et al. (2009). Biogeochemistry of nitrous oxide in groundwater in a forested ecosystem elucidated by nitrous oxide isotopomer measurements. *Geochimica et Cosmochimica Acta*, 73(11), 3115–3133. <https://doi.org/10.1016/j.gca.2009.03.022>
- Koster, J. R., Well, R., Tuzson, B., Bol, R., Dittert, K., Giesemann, A., et al. (2013). Novel laser spectroscopic technique for continuous analysis of N<sub>2</sub>O isotopomers—Application and intercomparison with isotope ratio mass spectrometry. *Rapid Communications in Mass Spectrometry*, 27(1), 216–222. <https://doi.org/10.1002/rcm.6434>
- Kraus, D., Weller, S., Klatt, S., Haas, E., Wassmann, R., Kiese, R., & Butterbach-Bahl, K. (2015). A new LandscapeDNDC biogeochemical module to predict CH<sub>4</sub> and N<sub>2</sub>O emissions from lowland rice and upland cropping systems. *Plant and Soil*, 386(1-2), 125–149. <https://doi.org/10.1007/s11104-014-2255-x>
- Lachouani, P., Frank, A. H., & Wanek, W. (2010). A suite of sensitive chemical methods to determine the  $\delta^{15}\text{N}$  of ammonium, nitrate and total dissolved N in soil extracts. *Rapid Communications in Mass Spectrometry*, 24(24), 3615–3623. <https://doi.org/10.1002/rcm.4798>
- Lewicka-Szczepak, D., Augustin, J., Giesemann, A., & Well, R. (2017). Quantifying N<sub>2</sub>O reduction to N<sub>2</sub> based on N<sub>2</sub>O isotopocules—Validation with independent methods (helium incubation and <sup>15</sup>N gas flux method). *Biogeosciences*, 14(3), 711–732. <https://doi.org/10.5194/bg-14-711-2017>
- Lewicka-Szczepak, D., Dyckmans, J., Kaiser, J., Marca, A., Augustin, J., & Well, R. (2016). Oxygen isotope fractionation during N<sub>2</sub>O production by soil denitrification. *Biogeosciences*, 13(4), 1129–1144. <https://doi.org/10.5194/bg-13-1129-2016>



- Lewicka-Szczepak, D., Well, R., Köster, J. R., Fuß, R., Senbayram, M., Dittert, K., & Flessa, H. (2014). Experimental determinations of isotopic fractionation factors associated with  $\text{N}_2\text{O}$  production and reduction during denitrification in soils. *Geochimica et Cosmochimica Acta*, 134, 55–73. <https://doi.org/10.1016/j.gca.2014.03.010>
- Li, C. S., Aber, J., Stange, F., Butterbach-Bahl, K., & Papen, H. (2000). A process-oriented model of  $\text{N}_2\text{O}$  and NO emissions from forest soils: 1. Model development. *Journal of Geophysical Research*, 105(D4), 4369–4384. <https://doi.org/10.1029/1999JD900949>
- Li, C. S., Frolking, S., & Frolking, T. A. (1992a). A model of nitrous oxide evolution from soil driven by rainfall events. 1. Model structure and sensitivity. *Journal of Geophysical Research*, 97(D9), 9759–9776. <https://doi.org/10.1029/92jd00509>
- Li, C. S., Frolking, S., & Frolking, T. A. (1992b). A model of nitrous oxide evolution from soil driven by rainfall events. 2. Model applications. *Journal of Geophysical Research*, 97(D9), 9777–9783. <https://doi.org/10.1029/92JD00510>
- Mariotti, A., Germon, J. C., Hubert, P., Kaiser, P., Letolle, R., Tardieu, A., & Tardieu, P. (1981). Experimental-determination of nitrogen kinetic isotope fractionation: Some principles; illustration for the denitrification and nitrification processes. *Plant and Soil*, 62(3), 413–430. <https://doi.org/10.1007/Bf02374138>
- Merbold, L., Werner, E., Jacqueline, S., Mark, Z., David, N., & Nina, B. (2014). Greenhouse gas budget ( $\text{CO}_2$ ,  $\text{CH}_4$  and  $\text{N}_2\text{O}$ ) of intensively managed grassland following restoration. *Global Change Biology*, 20(6), 1913–1928. <https://doi.org/10.1111/gcb.12518>
- Mohn, J., Guggenheim, C., Tuzson, B., Vollmer, M. K., Toyoda, S., Yoshida, N., & Emmenegger, L. (2010). A liquid nitrogen-free preconcentration unit for measurements of ambient  $\text{N}_2\text{O}$  isotopomers by QCLAS. *Atmospheric Measurement Techniques*, 3(3), 609–618. <https://doi.org/10.5194/amt-3-609-2010>
- Mohn, J., Gutjahr, W., Toyoda, S., Harris, E., Ibraim, E., Geilmann, H., et al. (2016). Reassessment of the  $\text{NH}_4\text{NO}_3$  thermal decomposition technique for calibration of the  $\text{N}_2\text{O}$  isotopic composition. *Rapid Communications in Mass Spectrometry*, 30(23), 2487–2496. <https://doi.org/10.1002/rcm.7736>
- Mohn, J., Steinlin, C., Merbold, L., Emmenegger, L., & Hagedorn, F. (2013).  $\text{N}_2\text{O}$  emissions and source processes in snow-covered soils in the Swiss Alps. *Isotopes in Environmental and Health Studies*, 49(4), 520–531. <https://doi.org/10.1080/10256016.2013.826212>
- Mohn, J., Tuzson, B., Manninen, A., Yoshida, N., Toyoda, S., Brand, W. A., & Emmenegger, L. (2012). Site selective real-time measurements of atmospheric  $\text{N}_2\text{O}$  isotopomers by laser spectroscopy. *Atmospheric Measurement Techniques*, 5(7), 1601–1609. <https://doi.org/10.5194/amt-5-1601-2012>
- Molina-Herrera, S., Grote, R., Santabarbara-Ruiz, I., Kraus, D., Klatt, S., Haas, E., et al. (2015). Simulation of  $\text{CO}_2$  fluxes in European Forest ecosystems with the coupled soil-vegetation process model "LandscapeDNDC". *Forests*, 6(12), 1779–1809. <https://doi.org/10.3390/f6061779>
- Molina-Herrera, S., Haas, E., Klatt, S., Kraus, D., Augustin, J., Magliulo, V., et al. (2016). A modeling study on mitigation of  $\text{N}_2\text{O}$  emissions and  $\text{NO}_3$  leaching at different agricultural sites across Europe using LandscapeDNDC. *Science of the Total Environment*, 553, 128–140. <https://doi.org/10.1016/j.scitotenv.2015.12.099>
- Mook, W. G. (2001). *Environmental isotopes in the hydrological cycle. Principles and applications*. Paris, France: Unesco.
- Oney, B., Henne, S., Gruber, N., Leuenberger, M., Bamberger, I., Eugster, W., & Brunner, D. (2015). The CarboCount CH sites: Characterization of a dense greenhouse gas observation network. *Atmospheric Chemistry and Physics*, 15(19), 11,147–11,164. <https://doi.org/10.5194/acp-15-11147-2015>
- Ostrom, N. E., Pitt, A., Sutka, R., Ostrom, P. H., Grandy, A. S., Huizinga, K. M., & Robertson, G. P. (2007). Isotopologue effects during  $\text{N}_2\text{O}$  reduction in soils and in pure cultures of denitrifiers. *Journal of Geophysical Research*, 112, G02005. <https://doi.org/10.1029/2006JG000287>
- Parton, W. J., Holland, E. A., Del Grosso, S. J., Hartman, M. D., Martin, R. E., Mosier, A. R., et al. (2001). Generalized model for  $\text{NO}_x$  and  $\text{N}_2\text{O}$  emissions from soils. *Journal of Geophysical Research*, 106(D15), 17,403–17,419. <https://doi.org/10.1029/2001JD900101>
- Rastetter, E. B., Kwiatkowski, B. L., & McKane, R. B. (2005). A stable isotope simulator that can be coupled to existing mass balance models. *Ecological Applications*, 15(5), 1772–1782. <https://doi.org/10.1890/04-0643>
- Ravishankara, A. R., Daniel, J. S., & Portmann, R. W. (2009). Nitrous oxide ( $\text{N}_2\text{O}$ ): The dominant ozone-depleting substance emitted in the 21<sup>st</sup> century. *Science*, 326(5949), 123–125. <https://doi.org/10.1126/science.1176985>
- Robertson, G. P., & Groffman, M. P. (2015). *Soil microbiology, ecology, and biochemistry. nitrogen transformations*. New York: Springer.
- Röckmann, T., Kaiser, J., Brenninkmeijer, C. A. M., & Brand, W. A. (2003). Gas chromatography/isotope-ratio mass spectrometry method for high-precision position-dependent  $\text{N}^{15}$  and  $\text{O}^{18}$  measurements of atmospheric nitrous oxide. *Rapid Communications in Mass Spectrometry*, 17(16), 1897–1908. <https://doi.org/10.1002/rcm.1132>
- Rosenkranz, P., Brüggemann, N., Papen, H., Xu, Z., Seufert, G., & Butterbach-Bahl, K. (2006).  $\text{N}_2\text{O}$ , NO and  $\text{CH}_4$  exchange, and microbial N turnover over a Mediterranean pine forest soil. *Biogeosciences*, 3(2), 121–133. <https://doi.org/10.5194/bg-3-121-2006>
- Schindlbacher, A., Zechmeister-Boltenstern, S., & Butterbach-Bahl, K. (2004). Effects of soil moisture and temperature on NO,  $\text{NO}_2$ , and  $\text{N}_2\text{O}$  emissions from European forest soils. *Journal of Geophysical Research*, 109, D17302. <https://doi.org/10.1029/2004JD004590>
- Shoun, H., Kim, D.-H., Uchiyama, H., & Sugiyama, J. (1992). Denitrification by fungi. *FEMS Microbiology Letters*, 94(3), 277–281. <https://doi.org/10.1111/j.1574-6968.1992.tb05331.x>
- Sprenger, M., Tetzlaff, D., & Soulsby, C. (2017). Soil water stable isotopes reveal evaporation dynamics at the soil-plant-atmosphere interface of the critical zone. *Hydrology and Earth System Sciences*, 21(7), 3839–3858. <https://doi.org/10.5194/hess-21-3839-2017>
- Stiess, M., Hundt, P., Tuzson, B., Riedi, S., Wolf, J., Peretti, R., et al. (2016). Dual-section DFB-QCLs for multi-species trace gas analysis. *Photonics*, 3(2), 24. <https://doi.org/10.3390/photonics3020024>
- Sutka, R. L., Adams, G. C., Ostrom, N. E., & Ostrom, P. H. (2008). Isotopologue fractionation during  $\text{N}_2\text{O}$  production by fungal denitrification. *Rapid Communications in Mass Spectrometry*, 22(24), 3989–3996. <https://doi.org/10.1002/rcm.3820>
- Sutka, R. L., Ostrom, N. E., Ostrom, P. H., Breznak, J. A., Gandhi, H., Pitt, A. J., & Li, F. (2006). Distinguishing nitrous oxide production from nitrification and denitrification on the basis of isotopomer abundances. *Applied and Environmental Microbiology*, 72(1), 638–644. <https://doi.org/10.1128/Aem.72.1.638-644.2006>
- Toyoda, S., Mutobe, H., Yamagishi, H., Yoshida, N., & Tanji, Y. (2005). Fractionation of  $\text{N}_2\text{O}$  isotopomers during production by denitrifier. *Soil Biology & Biochemistry*, 37(8), 1535–1545. <https://doi.org/10.1016/j.soilbio.2005.01.009>
- Toyoda, S., Yano, M., Nishimura, S. i., Akiyama, H., Hayakawa, A., Koba, K., et al. (2011). Characterization and production and consumption processes of  $\text{N}_2\text{O}$  emitted from temperate agricultural soils determined via isotopomer ratio analysis. *Global Biogeochemical Cycles*, 25, GB2008. <https://doi.org/10.1029/2009GB003769>
- Toyoda, S., & Yoshida, N. (1999). Determination of nitrogen isotopomers of nitrous oxide on a modified isotope ratio mass spectrometer. *Analytical Chemistry*, 71(20), 4711–4718. <https://doi.org/10.1021/ac9904563>



- Verhoeven, E., Barthel, M., Yu, L., Celi, L., Said-Pullicino, D., Sleutel, S., et al. (2019). Early season N<sub>2</sub>O emissions under variable water management in rice systems: Source-partitioning emissions using isotope ratios along a depth profile. *Biogeosciences*, 16(2), 383–408. <https://doi.org/10.5194/bg-16-383-2019>
- Wei, J., Ibraim, E., Brüggemann, N., Vereecken, H., & Mohn, J. (2019). First real-time isotopic characterisation of N<sub>2</sub>O from chemodenitrification. *Geochimica et Cosmochimica Acta*, 267, 17–32. <https://doi.org/10.1016/j.gca.2019.09.018>
- Well, R., Flessa, H., Xing, L., Ju, X. T., & Romheld, V. (2008). Isotopologue ratios of N<sub>2</sub>O emitted from microcosms with NH<sub>4</sub><sup>+</sup> fertilized arable soils under conditions favoring nitrification. *Soil Biology & Biochemistry*, 40(9), 2416–2426. <https://doi.org/10.1016/j.soilbio.2008.06.003>
- Werner, R. A., Bruch, B. A., & Brand, W. A. (1999). ConFlo III—An interface for high precision  $\delta^{13}\text{C}$  and  $\delta^{15}\text{N}$  analysis with an extended dynamic range. *Rapid Communications in Mass Spectrometry*, 13(13), 1237–1241. [https://doi.org/10.1002/\(Sici\)1097-0231\(19990715\)13:13<1237::Aid-Rcm633>3.0.Co;2-C](https://doi.org/10.1002/(Sici)1097-0231(19990715)13:13<1237::Aid-Rcm633>3.0.Co;2-C)
- Winther, M., Balslev-Harder, D., Christensen, S., Priemé, A., Elberling, B., Crosson, E., & Blunier, T. (2018). Continuous measurements of nitrous oxide isotopomers during incubation experiments. *Biogeosciences*, 15(3), 767–780. <https://doi.org/10.5194/bg-15-767-2018>
- WMO, & GAW. (2017). WMO greenhouse gas bulletin.
- Wolf, B., Kiese, R., Chen, W. W., Grote, R., Zheng, X. H., & Butterbach-Bahl, K. (2012). Modeling N<sub>2</sub>O emissions from steppe in Inner Mongolia, China, with consideration of spring thaw and grazing intensity. *Plant and Soil*, 350(1–2), 297–310. <https://doi.org/10.1007/s11104-011-0908-6>
- Wolf, B., Merbold, L., Decock, C., Tuzson, B., Harris, E., Six, J., et al. (2015). First on-line isotopic characterization of N<sub>2</sub>O above intensively managed grassland. *Biogeosciences*, 12(8), 2517–2531. <https://doi.org/10.5194/bg-12-2517-2015>
- Wu, X., Brüggemann, N., Gasche, R., Shen, Z., Wolf, B., & Butterbach-Bahl, K. (2010). Environmental controls over soil-atmosphere exchange of N<sub>2</sub>O, NO, and CO<sub>2</sub> in a temperate Norway spruce forest. *Global Biogeochemical Cycles*, 24, GB2012. <https://doi.org/10.1029/2009GB003616>
- Wunderlin, P., Mohn, J., Joss, A., Emmenegger, L., & Siegrist, H. (2012). Mechanisms of N<sub>2</sub>O production in biological wastewater treatment under nitrifying and denitrifying conditions. *Water Research*, 46(4), 1027–1037. <https://doi.org/10.1016/j.watres.2011.11.080>
- Yamamoto, A., Uchida, Y., Akiyama, H., & Nakajima, Y. (2014). Continuous and unattended measurements of the site preference of nitrous oxide emitted from an agricultural soil using quantum cascade laser spectrometry with intercomparison with isotope ratio mass spectrometry. *Rapid Communications in Mass Spectrometry*, 28(13), 1444–1452. <https://doi.org/10.1002/rcm.6916>
- Zhang, S., Fang, Y., & Xi, D. (2015). Adaptation of micro-diffusion method for the analysis of  $^{15}\text{N}$  natural abundance of ammonium in samples with small volume. *Rapid Communications in Mass Spectrometry*, 29(14), 1297–1306. <https://doi.org/10.1002/rcm.7224>
- Zhu, X., Burger, M., Doane, T. A., & Horwath, W. R. (2013). Ammonia oxidation pathways and nitrifier denitrification are significant sources of N<sub>2</sub>O and NO under low oxygen availability. *Proceedings of the National Academy of Sciences of the United States of America*, 110(16), 6328–6333. <https://doi.org/10.1073/pnas.1219993110>